MULTICOMPONENT CRYSTALS OF VANILLIC ACID

by

Célestine Nyingika Tshahwa

Student number: 219124094

Thesis submitted in fulfilment of the requirements for the degree

Master of Applied Sciences in Chemistry

Department Of Chemistry

Faculty of Applied Sciences

Cape Peninsula University of Technology

Supervisor: Prof. Ayesha Jacobs

Cape Town

2024

Declaration

I, Célestine Nyingika Tshahwa, hereby declare that the contents of this thesis represent my own work, and that the thesis has not previously been submitted for academic examination towards any qualification. Furthermore, it represents my own ideas and not necessarily those of the Cape Peninsula University of Technology.

Abstract

Vanillic acid (VA) was used to form multicomponent crystals with 4,4-bipyridine (4,4-BP), 4-dimethylaminopyridine (4DMAP), 2-amino-5-methylpyridine (A25MP), 2-amino-6-methylpyridine (A26MP), 2-aminopyridine (A2MP) and 4-aminopyridine (A4MP). Six compounds were prepared using the slow evaporation technique comprising one cocrystal, three salts and two salt hydrates. The compounds were characterised using FTIR spectroscopy, thermal analysis and powder X-ray diffraction. Crystal structures were determined using single crystal X-ray diffraction.

Some compounds were successfully prepared using the grinding procedure, while others were only partially converted.

Thermogravimetry was used for the salt hydrates to obtain the percentage water contained in the crystal structures.

Supramolecular interactions in the obtained crystal structures of the cocrystal, salts and salt hydrates are dominated by hydrogen bonding (O-H···O and O-H···N), whereas π-π stacking and C-H··· π interactions played a minor role in the packing arrangements of the new solid forms.

Acknowledgements

I would like to convey my deepest appreciation to my supervisor, Prof Ayesha Jacobs for being an incredible mentor. Thank you for the constant guidance, encouragement, patience and support throughout the last four years. I firmly believe that your supervision has been a key factor behind the wholesome learning process for me.

I would like to acknowledge and thank my parents, husband, and family for believing in me and encouraging me to pursue all my goals in life. I would never have gotten here without your help and encouragement. You never made time and distance seem like an obstacle; you were only a phone call away.

Thank you, God for your blessing.

Table Of Contents

Declaration i

Abstract ii

Acknowledgements iii

List Of Figures vii

List Of Tables xi

Abbreviations/Terms/Acronyms xiii

Atom colours xiv

CHAPTER 1: INTRODUCTION 1

1.1 Supramolecular chemistry 1

1.2 Crystal Engineering 1

1.3 Cocrystal 2

1.4 Interactions in multicomponent crystals 4

1.5 Applications of cocrystallization 5

1.6 Mechanochemistry 6

1.7 Vanillic acid 6

1.8 Problem statement 9

1.9 Research aims 10

REFERENCES 11

CHAPTER 2: EXPERIMENTAL METHODS AND MATERIALS 17

2.1 Materials 17

2.1.1 Main compound 17

2.1.2 Cocrystal formers 17

2.1.3 Solvents 19

2.2 Methods 19

2.2.1 Crystal Growth 19

2.2.2 Grinding 19

2.2.3 Thermal Analysis 20

2.2.4 Single Crystal X-Ray Diffraction 20

2.2.5. Powder X-ray Diffraction 21

2.2.6 Infrared (IR) Spectroscopy 21

2.2.7 Computing Packages 22

REFERENCES **23**
CHAPTER 3: COCRYSTAL OF VANILLIC ACID WITH 4,4-BIPYRIDINE **25**
3.1 Introduction 25
3.2 Vanillic acid with 4,4-bipyridine (VA·4,4-BP) 25
3.2.1 FTIR analysis 26
3.2.2 Thermal analysis 27
3.2.3 Powder X-ray Diffraction 28
3.2.4 Crystal structure of VA·4,4-BP cocrystal 29
3.3 Summary 32
REFERENCES **33**
CHAPTER 4: SALTS OF VANILLIC ACID **34**
4.1 Introduction 34
4.2 Vanillic acid and 4-dimethylaminopyridine (VA^-)($4DMAP^+$) 34
4.2.1 FTIR spectroscopy 35
4.2.2 Thermal analysis 36
4.2.3 Powder X-ray diffraction 37
4.2.4 Structure determination 38
4.3 Vanillic acid and 2-amino-5-methylpyridine ($2VA^-$)($2A25MP^+$) 41
4.3.1 FTIR spectroscopy 42
4.3.2 Thermal analysis 43
4.3.3 Powder X-ray Diffraction 44
4.3.4 Structure Determination 45
4.4 Vanillic acid and 2-amino-6-methylpyridine (VA^-)($A26MP^+$) 48
4.4.1 FTIR spectroscopy 49
4.4.2 Thermal analysis 51
4.4.3 Powder X-ray Diffraction 52
4.4.4 Structure determination 53
4.5 Summary 55
REFERENCES **57**
CHAPTER 5: SALT HYDRATES OF VANILLIC ACID **58**
5.1 Introduction 58
5.2 Vanillic acid and 2-aminopyridine ($3(VA^-)3(A2MP^+)\cdot H_2O$) 58

5.2.1 FTIR spectroscopy 59
5.2.2 Thermal analysis 60
5.2.3 Powder X-ray diffraction 62
5.2.4 Structure determination 62
5.3 Vanillic acid and 4-aminopyridine ($(VA^-)(A4MP^+)\cdot 2H_2O$) 67
5.3.1 FTIR spectroscopy 67
5.3.2 Thermal analysis 69
5.3.3 Powder X-ray diffraction 70
5.3.4 Structure Determination 71
5.4 Summary 76
REFERENCES **77**
CHAPTER 6: SUMMARY AND CONCLUSION **78**

List Of Figures

Figure 1.1: Illustration of supramolecular chemistry. 1

Figure 1. 2: Hydrogen bond geometry description. 5

Figure 1.3: Vanillic acid (VA). 5

Figure 2.1: Chemical structure of vanillic acid. 15

Figure 2.2: Chemical structures of the cocrystal formers. 17

Figure 3.1: Chemical structures used in this study. 24

Figure 3.2: Asymmetric unit of the VA·4,4BP structure. 25

Figure 3.3: FTIR spectra of VA·4,4-BP Neat ground product, VA, 4,4-BP and VA·4,4-BP cocrystal. 26

Figure 3.4: DSC curves of neat ground product of VA+ 4,4-BP (green), VA·4,4-BP Bulk crystal (blue), 4,4-BP (red) and VA (black). 27

Figure 3.5: Solvent assisted ground product (green), Bulk crystal (red), Calculated pattern of VA · 4,4-BP (blue), vanillic acid (purple), ground product (black). 28

Figure 3.6: Hydrogen bonds of VA·4,4-BP cocrystal. 30

Figure 3.7: Packing diagram of VA·4,4-BP. 31

Figure 4.1: Chemical structures used in this study. 33

Figure 4.2: Asymmetric unit of the (VA^-)(4DMAP$^+$) structure with all the hydrogen atoms shown for numbering clarity. 34

Figure 4.3: FTIR spectra of (VA^-)(4DMAP$^+$) (blue), VA (red) and 4DMAP (black). 35

Figure 4.4: DSC curves of (VA^-)(4DMAP$^+$) (yellow), 4DMAP (blue) and VA (red) and TG curve of (VA^-)(4DMAP$^+$) (black). 36

Figure 4.5: PXRD patterns of (VA^{-})(4DMAP^{+}) (gold), VA (purple), 4DMAP (green), bulk crystal (blue), solvent assisted ground product (red) and neat ground product (black). 37

Figure 4.6: Hydrogen bond of (VA^{-})(4DMAP^{+}) salt with some hydrogen atoms omitted for clarity. 39

Figure 4.7: Packing diagram of (VA^{-})(4DMAP^{+}) along [010] with hydrogen atoms omitted.40

Figure 4.8: Asymmetric unit of the ($2VA^{-}$)(2A25MP^{+}) structure with all the hydrogen atoms shown for numbering clarity. 40

Figure 4.9: FTIR spectra of ($2VA^{-}$)(2A25MP^{+}) (blue), VA(red) and A25MP(black). 42

Figure 4.10: DSC curves of VA (red), A25MP (blue) , ($2VA^{-}$)(2A25MP^{+}) (yellow) and TG of ($2VA^{-}$)(2A25MP^{+})(black). 43

Figure 4.11: PXRD patterns of ($2VA^{-}$)(2A25MP^{+}) (gold), VA (purple), A25MP (green), bulk crystal (blue), solvent assisted ground product (red) and ground product (black). 44

Figure 4.12: Hydrogen bond of $2(VA^{-})\cdot2(2A5MP^{+})$ salt with some hydrogen atoms omitted for clarity. 46

Figure 4.13: Packing diagram of ($2VA^{-}$)(2A25MP^{+}) along [001] with hydrogen atoms omitted. 47

Figure 4.14: Numbering scheme of the asymmetric unit of (VA^{-})(A26MP^{+}). 48

Figure 4.15: FTIR spectrums of (VA^{-})(A26MP^{+}) (blue), VA (red) and A26MP (black). 49

Figure 4.16: TG:(VA^{-})(A26MP^{+}) (black), DSC curves of VA (red), A26MP (blue) and (VA^{-})(A26MP^{+}) (yellow). 50

Figure 4.17: Calculated patterns of (VA^{-})(A26MP^{+}) (gold), VA (purple), ground product (green), A26MP (blue), bulk crystal (red), solvent assisted ground product (black). 51

Figure 4.18: Hydrogen bond of (VA^{-})(A26MP^{+}) salt with some hydrogen atoms omitted for clarity. 53

Figure 4.19: Packing diagram of (VA^{-})(A26MP^{+}) along [100] with some hydrogen atoms omitted. 53

Figure 5.1: Chemical structures used in this study. 56

Figure 5.2: Asymmetric unit of the $3(VA^{-})3(A2MP^{+})\cdot H_2O$ structure with all the hydrogen atoms shown for numbering clarity. 57

Figure 5.3: FTIR spectra of $3(VA^{-})3(A2MP^{+})\cdot H_2O$ (blue), A2MP (red) and VA (black). 58

Figure 5.4: Thermal analysis curves: DSC of VA (blue), A2MP (orange), $3(VA^{-})3(A2MP^{+})\cdot H_2O$ (green), TG: $3(VA^{-})3(A2MP+)\cdot H_2O$ (sky blue). 59

Figure 5.5: PXRD patterns of calculated pattern of $3(VA^{-})3(A2MP^{+})\cdot H_2O$ (yellow), VA (purple), A2MP (green), ground product (blue), bulk crystal (red), solvent assisted ground product (black). 60

Figure 5.6: Hydrogen bonding of $3(VA^{-})3(2AMP^{+})\cdot H_2O$. 63

Figure 5.7: Packing diagram of $3(VA^{-})\cdot 3(2AMP^{+})\cdot H_2O$ (hydrogens have been omitted for clarity). 64

Figure 5.8: Cavities in which water molecules are located. 64

Figure 5.9: Asymmetric unit of the $(VA^{-})(A4MP^{+})\cdot 2H_2O$ structure with all the hydrogen atoms shown for numbering clarity. 65

Figure 5.10: FTIR spectra of VA (black), A4MP (red) and $(VA^{-})(A4MP^{+})\cdot 2H_2O$ (blue). 67

Figure 5.11: DSC curves of Vanillic acid (blue), A4MP (orange), $(VA^{-})(A4MP^{+})\cdot 2H_2O$ (red) and TG curve of $(VA^{-})(A4MP^{+})\cdot 2H_2O$. 68

Figure 5.12: A4MP+VA calculated pattern (yellow), A4MP+VA bulk crystal (purple), VA (green), A4MP (blue), A4MP+VA solvent assisted ground product (red), A4MP+VA neat ground product (black). 69

Figure 5.13: Packing diagram of $(VA^{-})(A4MP^{+})\cdot 2H_2O$. 71

Figure 5.14: Cavities in which water molecules are located. 71

Figure 5.15: Hydrogen bonding of $(VA^{-})(A4MP^{+})\cdot 2H_2O$. 73

List Of Tables

Table 1.1: Cocrystals and salts with vanillic acid available in the CSD. 7

Table 2.1: Physical properties of the cocrystal formers and their pK_a values. 16

Table 2.2: Summary of solvents. 17

Table 3.1: FTIR positions and assignments for the peaks in VA and VA.4,4-BP. 26

Table 3.2: Thermal analysis data for VA·4,4-BP. 27

Table 3.3: Crystal data and refinement parameters of VA·4,4-BP. 28

Table 3.4: Geometrical data for hydrogen bond of VA·4,4-BP. 30

Table 4.1: FTIR positions and assignments of peaks for VA, (VA^-)($4DMAP^+$) and 4DMAP. 34

Table 4.2: Thermal analysis data of VA, 4DMAP and (VA^-)($4DMAP^+$). 35

Table 4.3: Crystal data and refinement parameters of the (VA^-)($4DMAP^+$) salt. 37

Table 4.4: Geometrical data for hydrogen bonds of (VA^-)($4DMAP^+$). 39

Table 4.5: FTIR positions and assignments of peaks in VA, A25MP and ($2VA^-$)($2A25MP^+$). 41

Table 4.6: Thermal analysis data of VA, A25MP and ($2VA^-$)($2A25MP^+$). 43

Table 4.7: Crystal data and refinement parameters of($2VA^-$)($2A25MP^+$) salt. 44

Table 4.8: Geometrical data for hydrogen bond of ($2VA^-$)($2A25MP^+$). 46

Table 4.9: FTIR positions and assignments of peaks in VA, A26MP and (VA^-)($A26MP^+$). 49

Table 4.10: Thermal analysis data of (VA^-)($A26MP^+$). 50

Table 4.11: Crystal data and refinement parameters of (VA^-)($A26MP^+$). 52

Table 4.12: Geometrical data for hydrogen bonds of (VA^-)($A26MP^+$). 54

Table 5.1:FTIR positions and assignments of peaks in VA, A2MP and $3(VA^-)3(A2MP^+)\cdot H_2O$. 57

Table 5.2: Thermal analysis data for $3(VA^-)3(A2MP^+)\cdot H_2O$. 59

Table 5.3: Crystal data and refinement parameters of the 3(VA^-)3($A2MP^+$)·H_2O salt. 61

Table 5.4: Geometrical data for hydrogen bond of 3(VA^-)3($A2MP^+$)·H_2O. 62

Table 5.5: FTIR positions and assignments of peaks in VA, A4MP and (VA^-)($A4MP^+$)·$2H_2O$. 66

Table 5.6: Thermal analysis data for (VA^-)($4AMP^+$)·$2H_2O$. 67

Table 5.7: (VA^-)($A4MP^+$)·$2H_2O$ crystal data. 69

Table 5.8: Geometrical data for hydrogen bond of (VA^-)($A4MP^+$)·$2H_2O$. 72

Abbreviations/Terms/Acronyms

4DMAP	4-dimethylaminopyridine
4,4-BP	4,4-bipyridine
A25MP	2-amino-5-methylpyridine
A26MP	2-amino-6-methylpyridine
A2MP	2-aminopyridine
A4MP	4-aminopyridine
a, b, c	unit cell axes
α	alpha interaxial angle between b and c
β	beta interaxial angle between a and c
CSD	Cambridge Structural Database
DSC	Differential Scanning Calorimetry
°	degree
FT-IR	Fourier transform infra-red
g	grams
g mol^{-1}	grams per mole
IR	infra-red
K	kelvin
min	minutes
mmol	millimoles
PXRD	Powder X-Ray diffraction
%	percentage
T	temperature
TGA	Thermogravimetric Analysis
VA	Vanillic acid
Z	number of formula units per cell
γ	gamma interaxial angle between a and b

Atom colours

Hydrogen

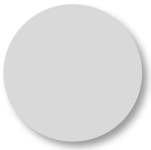

Carbon

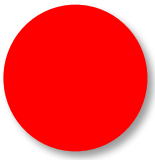

Oxygen

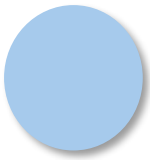

Nitrogen

CHAPTER 1: INTRODUCTION

1.1 Supramolecular chemistry

Supramolecular chemistry, defined as “chemistry beyond the molecule” is the chemistry of intermolecular bonds and molecular assemblages (Lehn, 1985). Noncovalent interactions between a "host" and a “guest” molecule form the origins of supramolecular chemistry (Lehn, 1973).

For their work on "host-guest" assemblies, Donald J. Cram, Jean-Marie Lehn, and Charles J. Pedersen shared the 1987 Nobel Prize in Chemistry. The emphasis was on several phenomena in supramolecular chemistry, such as metal coordination, hydrogen bonding, dipole-dipole interactions, and ion-dipole interactions, that are governed by certain noncovalent interactions between groups of molecules or ions (Lehn, 1996).

Supramolecular chemistry is crucial in diverse fields such as biology, physics, and chemistry.

Figure 1.1 illustrates a host-guest interaction. The nature of the target molecule must be carefully considered, and both host and guest molecules must work together to enable selective and effective recognition.

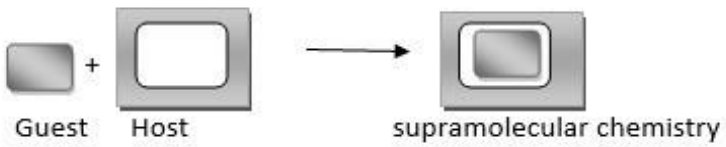

Figure1.1: Illustration of supramolecular chemistry.

1.2 Crystal Engineering

With the use of topochemical processes on cinnamic acid, Pepinsky (1955) and Schmidt (1971) presented the concept of crystal engineering. With the aid of X-ray crystallography, Schmidt and his colleagues worked in this newly emerging field to learn more about the fundamentals of organic molecule crystal packing with reference to crystalline cinnamic acid derivatives, how they interact in photodimerization reactions, and ultimately stability in structures.

The discovery of metal organics, organometallics, and organic solids in the 1900s gave rise to this field's propulsion (Desiraju, 1995). Since then, progress in crystal engineering has allowed for the planning of practical crystalline structures (Pepinsky, 1955; Schmidt, 1971; Etter,

1989). A definition of crystal engineering that has been used until today was given by Desiraju in 1989, who said crystal engineering is “the understanding of intermolecular interactions in the context of crystal packing and the utilization of such understanding in the design of new solids with desired physical and chemical properties”.

In crystal engineering, intermolecular interactions are essential. Noncovalent bonding, including π-π interactions, van der Waals forces, ionic or electrostatic connections, metal-ligand bonds, hydrogen bonding, and electrostatic forces, is crucial for comprehending crystal packing and self-assembly (Etter, 1989; Samlaska, 1994; Gupta, 1996).
Furthermore, intermolecular interactions produce the following element in crystals; self-assembly or molecular recognition which can be found in functional groups of molecules. Additionally, the intermolecular interactions with recurring patterns are called supramolecular synthons.

In organic chemistry, the synthon is defined as a fictive molecule, composed of functional groups capable of reacting and forming bonds. In the case of cocrystals, synthons are assemblages of several entities linked by noncovalent interactions which can stack up and give a structural order on a scale of a crystal (Pfeiffer, 2014). Additionally, Desiraju defined supramolecular synthons as “structural units within supermolecules which can be formed and/or assembled by known or conceivable synthetic operations involving intermolecular interactions” (Desiraju, 1995).
Supramolecular synthons are further classified as two basic types. Those that involve the same functional groups (homosynthons) such as two amides or two carboxylic acids and those that involve different but complementary functional groups (heterosynthons) such as an amide and a carboxylic acid group (Kitaigorodskii ,1973).
In crystal engineering, the synthons between acids, amides, and acid-amides are observed much more frequently than others, hence the identification of these frequently expressed motifs allow the understanding of the interactions necessary for cocrystallization.

1.3 Cocrystal

The first identified cocrystal was reported by Friedrich Wöhler in 1844. By mixing a solution of 1,4-benzoquinone, whose crystals are bright yellow, with metallic white crystals of hydroquinone, he obtained a green crystalline product. After analyzing the chemical

characteristics, Wöhler concluded that a combination of the two initial molecules was formed within the same cell, with a molar ratio of 1 to 1. Cocrystals are solid forms that have interested researchers for a long time. Like many fields of science and technology, the number of articles on the subject has been continuously increasing since the beginning of the 2000s. This interest in cocrystals has therefore continued to grow for several years. (Bernstein, 1995; Samlaska, 1994).

The term cocrystal first designated a single-phase crystalline material made up of several species linked together by noncovalent bonds. With this definition, hydrates and solvates, as well as all their polymorphs, can be considered subgroups of cocrystals. In these cases, a single species forms a crystal lattice comprising water or solvent molecules. In 2005, Aakeröy proposed restricting the name cocrystals to forms whose coformers are solid at room temperature. This criterion makes it possible to distinguish cocrystals from simple solvates or hydrates (Aakeröy, 2007).

Cocrystals and salts include two or more solid species in the same crystal and these multicomponent crystals are defined by the position of the proton between the acid and the base. Transfer of a proton from an acid to a base result in the formation of a salt.
Cocrystals are formed by mutual recognition based on the topography of coformers. They are held together by noncovalent interactions like hydrogen bonding, van der Waals interactions, or π-π interactions. Among these, hydrogen bonding is considered one of the most important interactions because of its high directionality and strength. Along with the interactions, the pK_a rule is often used to predict whether an acid-base pair of compounds will crystallize as a salt or a cocrystal.

Conventionally, the difference between the pK_a of the basic function and the pK_a of the interacting acid function serves as a criterion. The pK_a values of the main component and each coformer become essential in determining the formation of a cocrystal or a salt because most crystallization processes typically take place in solution. If the difference in pK_a between an acid and a base (pK_a base – pK_a acid) is more than 2-3, a salt will develop. Amines and carboxylic acids provide a huge number of the structures of cocrystals and salts that are now in use. In general, salts are generated when $\Delta pK_a > 3$, whereas cocrystals are formed when

$\Delta pK_a < 3$ (Tiekink, 2018). Additionally, Cruz Cabeza's investigations validate the above observations on the pK_a rule, indicating that ionized acid-base complexes are only detected for $\Delta pK_a > 4$, while non-ionized acid-base complexes are only observed for $\Delta pK_a < -1$ and there exists a possibility of salt formation for acid-base complexes with ΔpK_a values ranging from -1 to 4 (Cruz-Cabeza, 2012).

1.4 Interactions in multicomponent crystals

Over the past few years, cocrystal design has naturally emerged to modulate the characteristics of molecules of interest. To design a cocrystal, it is important to understand how the component molecules interact. For organic crystals, the most common noncovalent interactions are the hydrogen bond, van der Waals, dipole-dipole and halogen bond.

Hydrogen bonding can be categorised as a form of dipole–dipole attraction between the proton of a group A–H, where A is an electronegative atom, and one or more other electronegative atoms (Y) that contain a pair of nonbonded electrons (Desiraju, 2002). The A atom is called a donor, and the acceptor(s) are those which are not covalently linked to the hydrogen atom. The strength of a hydrogen bond can be discussed based on the distance between the donor and the acceptor, as well as with the angle formed by the three atoms involved (Figure 1.2). In crystallography, X-ray diffraction makes it possible to measure these data and thus evaluate the strength of interactions within the crystal (Steiner, 2002).

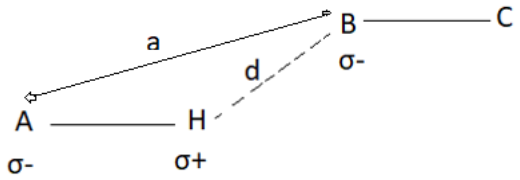

a = distance A…B
d = distance H…B
σ = charge of atom

Figure 1.2: Hydrogen bond geometry description.

Furthermore, IUPAC defines the hydrogen bond as an attractive connection between a hydrogen atom from a molecule or a molecular fragment A-H, where A is more electronegative than H, and an atom or a group of atoms in the same or different molecule, where bond formation is evident (Arunan et al, 2011).

Molecules in cocrystals can also be linked by π -π interactions or "π -stacking" interactions. IUPAC defines π -stacking as the inter- or intramolecular coplanar alignment of the aromatic groups of molecules induced by the interactional overlap of their orbitals (Jones & Ober, 2012).

1.5 Applications of cocrystallization

The principal motivation behind the development of cocrystallization is the ability to modify the physicochemical properties of compounds. Whereas the study and control of polymorphism focuses on the crystalline form and properties of a single compound, cocrystallization allows both the modification of the crystalline form, and the combination of properties specific to several molecules. Properties such as water solubility, hygroscopicity, as well as mechanical, optical, or electrical properties of crystalline compounds can be modified by cocrystallization (Chow & Chen, 2012; Feng & Wang, 2013).

Cocrystals and salts are used in the pharmaceutical industry to improve drug properties such as solubility, permeability, and dissolution rate, which have a direct impact on hygroscopicity, bioavailability, and photo-stability (Tiekink & Zukerman, 2018). Furthermore, cocrystallization is used to combine the pharmaceutical properties of several active molecules, thus this idea of formulation in a single phase was exploited by Évora and Castro in obtaining the cocrystal formed by pyrazinamide and diflunisal which is a design of a multicomponent phase with complementary pharmacological properties. This encourages synergy between the different actions of the compounds (Évora & Castro, 2011). Cocrystallization is also used in structural biology for the resolution of protein-ligand complexes. Likewise in organic chemistry, it is used as a conformational analysis tool (Pfeiffer, & Fowler, 2014). This technique is often used to obtain structural data of cocrystals.

Cocrystallization is also used to form specific interactions between two species thus allowing extraction and purification of a compound of interest in a reactor with the cocrystal obtained by filtration (Billot & Hosek, 2013). Finally, in the food sector, cocrystallization is also used to enhance the flavour of food additives by cocrystallizing them with certain ingredients, like vanillin or vanillic acid, to balance or conceal undesirable qualities like acidity and bitterness (Xu & Li, 2015).

1.6 Mechanochemistry

Mechanochemistry is chemical synthesis facilitated or sustained by mechanical force (James et al, 2012). Used since antiquity in organic synthesis, mechanochemistry, rapidly established itself as an effective method for producing therapeutic compounds. Thus, it is a growing subject, in part because it does not require high temperature or pressure and allows many different combinations to be tested at the same time in a tool such as a ball mill or simply by using a mortar and pestle.

IUPAC defines mechanochemical reactions as "those caused by the direct absorption of mechanical energy (Baláž et al, 2012), for example under the action of shearing, friction or grinding, neat grinding or liquid-assisted grinding (also known as kneading) are commonly used methods for preparing cocrystals by mechanochemistry (Friscic, 2012).

Neat grinding, which involves grinding two or more dry cocrystallized components without a solvent, was a pioneering process in mechanochemistry. Arthur R. Ling used this method in 1893 to make the first hydrogen-bonded cocrystal, quinhydrone (Ling, 1893).

The first case of liquid assisted grinding which consists of adding a small amount of a liquid during the grinding process was reported by Shan et al in 2002 to demonstrate that adding small amounts of appropriate solvent(s) can significantly improve the kinetics of cocrystal formation (Shan et al, 2002).

1.7 Vanillic acid

A derivative of benzoic acid called vanillic acid (4-hydroxy-3-methoxybenzoic acid), Figure 1.3, is used as a flavouring agent. It is vanillin that has been oxidized and is created when vanillin is transformed into ferulic acid. It is of great importance regarding food and pharmaceutical industries; as flavouring agents in foods, including condiments and seasonings, and in drug products, or related to the manufacturing of drugs.

Studies have reported that vanillic acid can be used as an antioxidant and anti-inflammatory agent in vitro and ex vivo in human immune cells and non-cellular models (Mangeria et al., 2025), and furthermore vanillic acid can be used to reduce synovitis and pain-related behaviours in a rat model of knee osteoarthritis (KOA) which is one of the most frequent chronic degenerative bone disorders and joint discomfort (Ma et al., 2021).

Vanillic acid ($C_8H_8O_4$) has an appearance of a white to yellow powder or crystals. It has a molar mass of 168.148 $g \cdot mol^{-1}$, melting point of 210 to 213 °C and contains various functional groups (-COOH, -OH and $–OCH_3$) capable of forming hydrogen bonds (Lesage-Meessen, 1996).

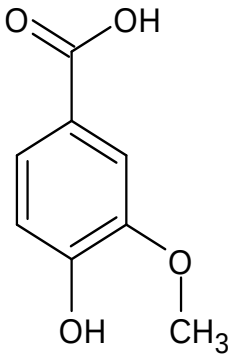

Figure 1.3:Vanillic acid (VA)

A search of the latest Cambridge Structural Database (CSD version 5.45, June 2024 updates) (Groom & Bruno, 2016) gave 32 cocrystal structures, 5 salt hydrates and 1 salt containing vanillic acid. Kozlevcar and Odlazek reported two copper (II) coordination compounds with vanillic acid (Kozlevcar & Odlazek, 2005). Suresh and Minkov reported a 1:1 cocrystal of vanillic acid with a sulfonamide named sulfamethizole (Suresh & Minkov, 2015). In 2013 Suresh and Goud reported a 1:1 co-crystal of vanillic acid with a diterpenoid lactone named andrographolide (Suresh & Goud, 2013). Dalpiaz et al. reported in 2017 a cocrystal formed with carbamazepine and vanillic acid (CBZ-VAN) that showed an increase in solubility compared to the carbamazepine alone (Dalpiaz & Ferretti, 2017). Cocrystals of vanillic acid with riluzole (Balvant & Sridhar, 2018) and isoniazid (Battini & Maddileti, 2014) have also been reported.

A series of cocrystals containing vanillic acid was reported by Jacobs & Amombo Noa with caffeine (VA·2CAF), theophylline(2VA·THP), nicotinamide (VA·NAM) and acridine (VA·ACR). Cocrystal hydrates of vanillic acid with theobromine (VA·THB·$2H_2O$) and isonicotinamide (2VA·2INM·$2H_2O$) were also obtained (Jacobs & Amombo Noa, 2014).

Cocrystals and salts of vanillic acid and vanillin with amines have also been reported (Amombo Noa & Mehlana, 2018). Vanillin formed a cocrystal with isonicotinamide, and a cocrystal hydrate with theobromine. Binary cocrystals of vanillic acid with isonicotinamide, hexamethylenetetramine, phenazine, and pyrazine-N-oxide were obtained. They also

described a ternary cocrystal that resulted from a 1: 1: 1 ratio of vanillic acid, caffeine and nicotinamide. Salt hydrates were also formed between piperazine, and 1,4-diazabicyclo[2.2.2]octane with vanillic acid.

Angevine and Benedict reported a cocrystal formed between vanillic acid and 4,4-bipyridine in a 1:1 ratio with the resulting cocrystal possessing monoclinic symmetry at 90 K (Angevine & Benedict, 2022). In their studies, Krishna et al. showed that by changing the crystal packing through cocrystallization, one can change the mechanical properties of the studied compounds, and this has been illustrated in cocrystals of vanillin isomers.

The hydrogen bond acceptor in vanillic acid is the methoxy group, while the strongest hydrogen bond donor is the carboxylic acid group, which is followed by the hydroxyl group. These characteristics together with its role in the food and pharmaceutical industries make vanillic acid an interesting compound for crystal engineering studies.

Common synthons formed by vanillic acid in the CSD database were acid-amide heterosynthons, alcohol-pyridine heterosynthons and acid-acid homosynthons. All the cocrystal coformers contain at least one nitrogen atom and seven of them were pyridines. The table below summarises all the cocrystals and salts obtained with vanillic acid from the CSD and their calculated predicted values of ΔpK_a using Chemspider.

Table 1.1: Cocrystals and salts with vanillic acid available in the CSD.

Cocrystal former	**ΔpK_a**	**Cocrystal or salt formation**
Caffeine	-5.32	Cocrystal
Caffeine-nicotinamide	-5.32; -0.53	Cocrystal
Theobromine	-5.3	Cocrystal/Cocrystal hydrate
Isoniazid	-0.9	Cocrystal
Isonicotinamide	-0.71	Cocrystal/Cocrystal hydrate
Nicotinamide	-0.53	Cocrystal
Riluzole	-0.49	Cocrystal
Sulfamethizole	0.45	Cocrystal
4,4'-bipyridine	1.09	Cocrystal
Pyrazine-N-oxide	1.46; 0.49	Cocrystal
Phenazine	1.46	Cocrystal
Hexamethylenetetramine	1.72	Cocrystal
Acridine	1.99	Cocrystal
Piperazine	5.4	Salt hydrate
1,4-diazabicyclo[2.2.2]octane	5.6	Salt hydrate
Lactone	9.34	Cocrystal
Carbamazepine	11.8	Cocrystal

1.8 Problem statement

The choice of appropriate components in building a new solid form is still difficult since crystal engineering principles and hydrogen bonding rules are the principal design elements for the preparation of cocrystals with predictable and robust supramolecular synthons (Desiraju, 1995). The preparation of new cocrystal forms of the same component with new physicochemical properties represents a challenge to chemists and a chance to introduce new solid forms with immediate applications in diverse areas such as pharmaceuticals, agrochemicals and synthetic chemistry. In this study, multicomponent crystals of vanillic acid were investigated. Vanillic acid was chosen due to the functional groups (-COOH, -OH and –OCH_3) to form salts/cocrystals with pyridines/aminopyridines to determine which supramolecular synthons would form. Furthermore, there are not many organic salts of vanillic acid in the literature as discussed in 1.7 and this study contributes towards the structural landscape of vanillic acid

1.9 Research aims

The ability of cocrystallization to alter the physicochemical characteristics of the pure chemical component without changing its chemical structure makes it significant. Crystallization designs a new crystal structure without changing any covalent bonds of the starting components. The main objective of the study was to obtain multicomponent crystals of vanillic acid with selected nitrogen containing compounds (pyridines). The multicomponent crystals were characterized using established techniques. This study utilised the selected compounds to form a cocrystal or salt depending on the pK_a differences between molecules. Different minor studies led to the achievement of the objectives, such as:

- The study of the different preparation methods of the compounds, which include neat grinding experiments, solvent assisted grinding experiments and solvent evaporation techniques.

For every combination of acid and base, the same crystallization technique was applied under the same circumstances. Since alcohols are well-known solvents in the formation of cocrystals, propan-2-ol and ethanol, as well as mixtures of ethanol and propan-2-ol, were selected as the solvents.

REFERENCES

Aakeröy, C.B. and Salmon, D.J. 2005. Building co-crystals with molecular sense and supramolecular sensibility. *CrystEngComm* 7 (72): 439–448.

Aakeröy, C. B.; Fasulo, M. E.; Desper, J. 2007. Cocrystal or salt: does it really matter? *Mol. Pharm.* 4(3): 317–322.

Aitipamula, S.; Banerjee, R., Bansal, A.K.; Biradha, K., Cheney, M.L.; Choudhury, A.R., Desiraju, G.R., Dikundwar, A.G., Dubey, R., Duggirala, N. and Ghogale, P.P. 2012. Polymorphs, salts, and cocrystals: *Cryst. Growth & Des*., 12(5): 2147-2152.

Arunan, E.; Desiraju, G.R.; Klein, R.A.; Sadlej; Joanna, S.; Steve, S.; Ibon, A.; Clary, D.C.; Crabtree, R.H.; Dannenberg, J.J.; Hobza, P.; Kjaergaard, H.G.; Legon, A.C.; Mennucci, B.; & Nesbitt, D.J. 2011. Definition of the hydrogen bond (IUPAC Recommendations 2011), *Pure and Applied Chemistry*, vol. 83, 8: 1637-1641.

Amombo, Noa, F. M. A. and Mehlana, G. 2018. Co-crystals and salts of vanillic acid and vanillin with amines. *CrystEngComm*, 20(7): 896–905.

Baláž, P.; Achimovičová, M.; Baláž, M.; Billik, P.; Cherkezova-Zheleva, Z.; Criado, J.M.; Delogu, F.; Dutková, E.; Gaffet, E.; Gotor, F.J.; et al. 2013. Hallmarks of Mechanochemistry: From Nanoparticles to Technology. *Chem. Soc. Rev*., 42: 7571–7637.

Bernstein, Davis, R.E, Shimoni, L., Chang, N.L. 1995. Patterns in hydrogen bonding–functionality and graph set analysis in crystals. *Angew. Chem. Int*. *Ed.* 34: 1555–1573.

Billot, P.; Hosek, P.; Perrin, M.-A. 2013. Efficient purification of an active pharmaceutical ingredient via cocrystallization: from thermodynamics to scale-up. *Org. Process Res. Dev*. 17 (3): 505– 511.

Cavitands, Gibb, B. C. 2004. Encyclopedia of Supramolecular Chemistry Eds. Atwood, J. & Steed, J., Marcel Dekker, p219-222.

Caracelli,I.; Haiduc,I.; Zukerman-Schpector J.; Tiekink E.R.T. 2016. in Aromatic interactions: frontiers in knowledge and application, eds D. W. Johnson and F. Hof, Abingdon: *Royal Society of Chemistry*, p. 98–123.

Chow, S. F.; Chen, M.; Shi, L.; Chow, A. H. L.; Sun, C. 2012. Simultaneously improving the mechanical properties, dissolution performance, and hygroscopicity of ibuprofen and flurbiprofen by cocrystallization with nicotinamide. *Pharm. Res*. 29 (7): 1854–1865.

Civolani, C.; Barghini, P.; Roncetti, A.R.; Ruzzi, M.; Schiesser, A. 2000. Bioconversion of ferulic acid into vanillic acid by means of a vanillate-negative mutant of Pseudomonas fluorescens strain BF13. *Appl Environ Microbiol*. 66: 2311–2317.

Clyburne. J. A. C, Hamilton. T & Jenkins. H. A. 2001. *Cryst. Eng.* 4, 1-9.

Corpinot, MK & Bučar, DK. 2019. A practical guide to the design of molecular Crystals. *Cryst. Growth & Des.,*19(2): 1426-1453.

Cram, D. J. 1988. The Design of Molecular Hosts, Guests, and Their Complexes. *Angew. Chem. Int*. *Ed.* 27, 109.

Cruz-Cabeza, A. J. 2012. Acid-base crystalline complexes and the p*K*a rule. *CrystEngComm*, 14(20), 6362–6365.

Desiraju, G.R. 1995. Supramolecular synthons in crystal engineering–a new organic synthesis. *Angew. Chem. Int*. *Ed. Engl*. 34: 2311–2327.

Desiraju, G.R., Vittal, J.J. and Ramanan, A., 2011. Crystal engineering: a textbook. World Scientific.

Desiraju, G. R. 2013. Crystal Engineering: From Molecule to Crystal. *J. Am. Chem. Soc.* 135 (27): 9952–9967.

Desiraju, G.R. 2002. Hydrogen bridges in crystal engineering: interactions without borders, *Acc. Chem. Res*. 35(7): 565–573.

Edward R. T. Tiekink, Julio Zukerman-Schpector (Eds.) Multi-Component Crystals, 2018.

Etter, M.C, MacDonald, J.C. & Bernstein, J. 1990. Graph-set analysis of hydrogen bond patterns in organic crystals, *Acta Cryst*. B46: 256–262.

Etter M.C., Frankenbach G.M. 1989. Hydrogen-bond directed co-crystallization as a tool for designing acentric organic solids. *Chem. Mater.* 1:10–12.

Évora, A. O. L.; Castro, R. A. E.; Maria, T. M. R.; Rosado, M. T. S.; Ramos Silva, M.; Matos Beja, A.; Canotilho, J. and Eusébio, M. E. S. 2011. Pyrazinamide-diflunisal: a new dual-drug co-crystal. Cryst. Growth & Des. 11(11): 4780–4788.

Feng, Q.; Wang, M.; Dong, B.; He, J. and Xu, C. 2013. Regulation of arrangements of pyrene fluorophores via solvates and cocrystals for fluorescence modulation. *Cryst. Growth & Des.* 13 (10): 4418–4427.

Fujita, M. 2003. Molecular self-assembly: organic versus inorganic approaches (Vol. 96). Springer.

Friscic, T. 2012. Supramolecular concepts and new techniques in mechanochemistry: cocrystals, cages, rotaxanes, open metal-organic frameworks. *Chem. Soc. Rev*. 41 (9): 3493−3510.

Goodman, L.S.; Gilman, A.; Hardman, J.G.; Gilman, A.G.; Limbird, L.E. 1996. Goodman & Gilman's the Pharmacological Basis of Therapeutics. New York: McGraw-Hill.

Groom, C.R., Bruno, I.J., Lightfoot, M.P. and Ward, S.C. 2016. The Cambridge Structural Database. *Acta Cryst. B*, 72: 171-179.

Jacobs, A., and Amombo Noa, F. M. 2015. Co-crystals and co-crystal hydrates of vanillic acid. *CrystEngComm*, 17(1): 98–106.

Jeffrey, G.A.; Jeffrey, G.A. 1997.An Introduction to Hydrogen Bonding; Oxford University Press: New York, NY, USA,Volume 12.

James, S. L.; Adams, C. J.; Bolm, C.; Braga, D.; Collier, P.; Friš čić ,T.; Grepioni, F.; Harris, K. D. M.; Hyett, G.; Jones, W.; Krebs, A.; Mack,J.; Maini, L.; Orpen, A. G.; Parkin, I. P.; Shearouse, W. C.; Steed, J. W.;Waddell, D. C. 2012. Mechanochemistry: opportunities for new and cleanersynthesis: *Chem. Soc. Rev.*, 41: 413−447.

Jones, R. G.; Ober, C. K.; Hodge, P.; Kratochvíl, P.; Moad, G. and others. 2013. Terminology for self-assembly and aggregation of polymers (IUPAC Provisional Recommendations).

Krishna, G.R.; Shi, L.; Bag, P.; Sun, C.; Reddy, C.M . 2015. Correlation Among Crystal Structure, Mechanical Behavior, and Tabletability in the Co-Crystals of Vanillin Isomers. *Cryst Growth* & *Des.* 15 (4): 1827–1832.

Kitaigorodskii, A. I. 1961. Organic Chemical Crystallography. *New York: Consultants Bureau*.

Kitaigorodskii, A. I. 1973. Molecular Crystals and Molecules. *New York: Academic Press*.

Lehn, J., 1985. Supramolecular chemistry: receptors, catalysts, and carriers. Science, Volume 227, p. 849.

Lehn, J. M. 1973. Struct. Bonding. 16, 1.

Lehn, J. M. 1978. Cryptates–chemistry of macropolycyclic inclusion complexes. *Acc. Chem. Res*. 11: 49–57.

Lehn, J.M., 2002. Supramolecular chemistry and self-assembly special feature: Toward complex matter: supramolecular chemistry and self-organization', Proc. Nat. Acad. Sci. USA, 99, 4763–4768.

Lehn, J. M. 1988. *Angew. Chem. Int. Ed.*27, 89.

Lehn, J. M. 1988. *Angew. Chem., Int.* 112, 90.

Lehn, J. M. 1990. *Angew. Chem. Int. Ed.* 29, 1304.

Lehn, J. M. 1995. Supramolecular Chemistry: Concepts and Perspectives.

Lehn, J.M. 1996. Supramolecular Chemistry and Chemical Synthesis. In: Chatgilialoglu, C., Snieckus, V. (eds) Chemical Synthesis. NATO ASI Series, vol 320. Springer, Dordrecht.

Lehn, J. M. 1988. VCH, Weinhein. *Angew. Chem. Int. Ed.* 27, 89.

Lesage-Meessen, L.; Delattre, M.; Haon, M.; Thibault, J.F.; Ceccaldi, B.C.; Brunerie, P.; Asther, M. 1996. A two-step bioconversion process for vanillin production from ferulic acid combining Aspergillus niger and Pycnoporus cinnabarinus. *J. Biotechnol.* 50: 107– 113.

Ling, A. R.; Baker, J. L. XCVI. 1893. Halogen derivatives of quinone. Part III. Derivatives of quinhydrone. *J. Chem. Soc., Trans*. 63: 1314–1327.

Ma, Z.; Huang, Z.; Zhang, L.; Li, X.; Xu, B.; Xiao, Y.; et al. 2021. Vanillic Acid Reduces Pain-Related Behavior in Knee Osteoarthritis Rats Through the Inhibition of NLRP3 Inflammasome-Related Synovitis. *Front Pharmacol*.11:1–9.

Magiera, A.; Kołodziejczyk-Czepas, J.; Olszewska, M.A. 2025. Antioxidant and Anti-Inflammatory Effects of Vanillic Acid in Human Plasma, Human Neutrophils, and Non-Cellular Models In Vitro. *Molecules*. 30: 467.

Moore, T. S.; Winmill, T. F. 1912. The state of amines in aqueous solution". *J. Chem. Soc.* 101: 1635.

Pfeiffer, C. R.; Fowler, D. A.; Teat, S. and Atwood, J. L. 2014.Cocrystallization of pyrogallol[4]arenes with 1-(2-pyridylazo)-2-naphthol. *CrystEngComm*. 16 (47): 10760–10773.

Pauling, L. 1960. The nature of the chemical bond and the structure of molecules and crystals; an introduction to modern structural chemistry (3rd ed.). Ithaca (NY): Cornell University Press. p. 450.

Pepinsky, R. 1955. Crystal engineering: New concepts in crystallography. *Phys Rev*, 100: 971–971.

Pfeiffer, C. R.; Fowler, D. A.; Teat, S.; Atwood, J. L. 2014.Cocrystallization of pyrogallol[4]arenes with 1-(2-pyridylazo)-2-naphthol. *CrystEngComm* , 16 (47): 10760–10773.

Ramon, G., Davies K., Nassimbeni L.R. 2014. Structures of benzoic acids with substituted pyridines and quinolines: salt versus co-crystal formation. *CrystEngComm,* 16: 5802–5810.

Rebek, J. 1987. Model studies in molecular recognition. *Science.* 235 (4795): 1478–84.

Rodríguez-Spong, B.; Price, C. P.; Jayasankar, A.; Matzger, A. J.; Rodríguez-Hornedo, N. 2004. General principles of pharmaceutical solid polymorphism: *Adv. Drug Delivery Rev.* 56: 241-74.

Samlaska, C.P.; Winfield, E.A. *J. Am. Acad. Dermatol.* 1994. 30, 603-621.

Shan, N.; Toda, F.; Jones, W. 2002. Mechanochemistry and co-crystal formation: effect of solvent on reaction kinetics. *Chem. Commun.* No. 20: 2372−2373.

Steiner, T. 2002.The hydrogen bond in the solid state. *Angew. Chem. Int*. *Ed.* 41 (1), 48–76

Suresh, K., Goud, N. R., and Nangia, A. 2013. Andrographolide: solving chemical instability and poor solubility by means of cocrystals. *Chem. Asian J.*8(12): 3032– 3041.

Suresh, K., Minkov, V. S., Namila, K. K., Derevyannikova, E., Losev, E., Nangia, A. and Boldyreva, E. V. 2015. Novel synthons in sulfamethizole cocrystals: structure-property relations and solubility. *Cryst. Growth & Des.*15(7): 3498–3510.

Silverman, R.B.; Holladay, M.W., The Organic Chemistry of Drug Design and Drug Action (Third Edition), 2014.

Salonen, L. M.; Ellermann, M.; Diederich, F. 2011.Aromatic Rings in Chemical and Biological Recognition: Energetics and Structures. *Angew. Chem. Int*. *Ed.* 50 (21): 4808–4842.

Schmidt, G.M. 1971. Photodimerization in the solid state. *J Pure Appl. Chem.* 27: 647– 678.

Sherrill, C. D. 2013.Energy Component Analysis of π Interactions. *Acc. Chem. Res*. 46 (4): 1020–1028.

Swapna, B.; Maddileti; D., Nangia, A. 2014. Cocrystals of the tuberculosis drug isoniazid: Polymorphism, isostructurality, and stability. *Cryst Growth & Des*. 14(11): 5991–6005.

Tiekink, E.; Zukerman-Schpector, J. De Gruyter, 2017, Multi-Component Crystals. Synthesis, Concepts, Function.

Trask, A.V; Jones, W. 2005. in Organic solid-state reactions, ed. F. Toda, Springer Berlin Heiderlberg, Berlin, Heidelberg, pp.41-70.

Xu, J., Xu, H., Liu, Y., He, H. and Li, G. 2015. Vanillin-induced amelioration of depression-like behaviors in rats by modulating monoamine neurotransmitters in the brain. *Psychiatry Research, 225*(3), 509–514.

Zhang, M.; Lou, B.; Huang, X.; Huang, Y. 2018. Crystal structure of 9,10-dimethoxy-5,6-dihydro-[1,3]dioxolo[4,5-g]isoquinolino[3,2-a]isoquinolin-7-ium chloride-4hydroxy-3-

methoxybenzoic acid-water (2/1/5), $C_{48}H_{54}N_2Cl_2O_{17}$. *Z. fur Krist. - New Cryst. Struct.* 233(2): 291–293.

CHAPTER 2: EXPERIMENTAL METHODS AND MATERIALS

2.1 Materials

2.1.1 Main compound

Vanillic acid also known as 4-hydroxy-3-methoxybenzoic acid is a phenolic acid with functional groups (-COOH and -OH) that can form hydrogen bonds with donor or acceptor molecules. Acids can transfer their proton to a base to generate salts, which in turn create charge-assisted hydrogen bonds. This phenolic acid with an appearance of white to yellow powder or crystals, has a molar mass of 168.148 g mol^{-1}, and the melting point of 210 to 213 °C (483 to 486 K). Vanillic acid was purchased from Sigma-Aldrich and has a purity of approximatively 99%, so no further purification was needed.

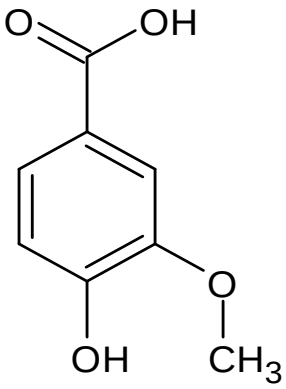

Figure 2.1: Chemical structure of vanillic acid.

2.1.2 Cocrystal formers

The experimental objective was to obtain multicomponent crystals by using selected nitrogen containing compounds (pyridines) that have abilities to form hydrogen bonds with vanillic acid. Thus a selection of pyridines were chosen as cocrystal formers, namely 2-aminopyridine (2AMP), 4-aminopyridine (4AMP), 4-dimethylaminopyridine (4DAMP), 4,4-bipyridine (4,4-BP), 2-amino-5-methylpyridine (A25MP) and 2-amino-6-methylpyridine (A26MP). Physical properties of the cocrystal formers and their pK_a values are given in Table 2.1. The chemical structures of the cocrystal formers are represented in Figure 2.2.

Table 2.1: Physical properties of the cocrystal formers and their pK_a values.

Name, origin and purity	**Formula**	**M_r (g mol^{-1})**	**Bp (°C)**	**Mp (°C)**	**pK_a**
2-Aminopyridine, Sigma-Aldrich,99%	$C_5H_6N_2$	94.1	204-210	54-58	6.84
4-Aminopyridine, Sigma-Aldrich, ≥ 99%	$C_5H_6N_2$	94.1	273	155-158	8.95
4-Dimethylaminopyridine Sigma-Aldrich, ≥ 99%	$C_7H_{10}N_2$	122.2	162	108-110	8.78
4,4-Bipyridine, Sigma-Aldrich, 99%	$C_{10}H_8N_2$	156.2	305	109-112	5.25
2-Amino-5-methylpyridine, Sigma-Aldrich, 99%	$C_6H_8N_2$	108.1	227	76-77	7.68
2-Amino-6-methylpyridine, Sigma-Aldrich, 98%	$C_6H_8N_2$	108.1	208-209	40-44	7.6

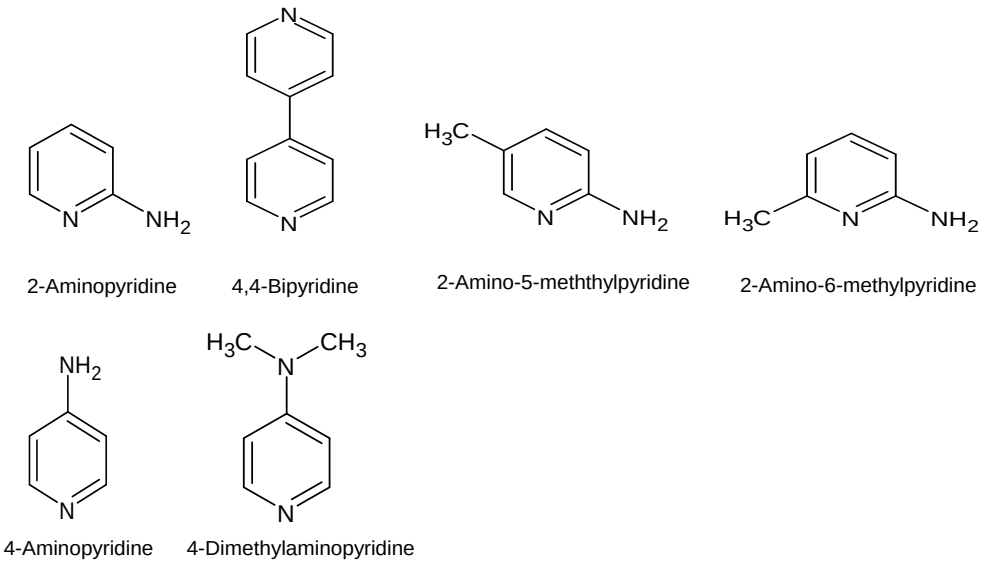

Figure 2.2: Chemical structures of the cocrystal formers.

2.1.3 Solvents

Solvents listed in Table 2.2 were purchased from Merck (Pty) Ltd and were used as is.

Table 2.2: Summary of solvent properties.

Name	Formula	Mass ($g\ mol^{-1}$)	Melting point(°C)	Boiling point(°C)	Density ($g\ cm^3$)
Ethanol	C_2H_6O	46.1	-117.3	78.5	0.79
Propan-2-ol	C_3H_8O	60.1	-89	82.6	0.785

2.2 Methods

2.2.1 Crystal Growth

Various methods exist for crystallization of small molecules such as the slow cooling method, diffusion method, slow evaporation, and other techniques (Laudise, 1970). The slow evaporation method was used in this study in all crystallizations. The new solid form was obtained by dissolving the target compound and cocrystal former in a 1:1 molar ratio in different chosen organic solvents, the mixture was then placed on the hot plate and stirred to ensure complete dissolution and homogenization of the solution. Solvent selection was based on their ability to completely dissolve the solid mixture. The mixture was then left at ambient temperature to allow the slow evaporation of the solvent or solvent mixture and crystal formation was observed after a few days. Further details are given in the relevant chapters.

2.2.2 Grinding

The target compound (vanillic acid) and selected cocrystal formers were ground together manually with and without solvent using a mortar and pestle. In the case of neat grinding, an equimolar mixture of the initial powders is placed in a mortar, then pounded for 25 minutes. For solvent grinding, the same procedure as above was followed with the addition of a few drops of the appropriate solvent. After grinding, the powder was collected and analysed using powder X-ray diffraction (PXRD).

2.2.3 Thermal Analysis

Thermal analysis is a group of techniques that measures a selected physical property of a sample while the sample is heated or cooled (Brown, 2001). The thermal decomposition profiles of the resulting compounds were determined by the thermal analytical techniques of differential scanning calorimetry (DSC) and thermogravimetry (TG).

- ***Differential Scanning Calorimetry (DSC)***

A Perkin-Elmer Pyris 6 system was used for these analyses, which were carried out under nitrogen purge gas at a flow rate of 20 mL min^{-1}. Sample masses of 2 to 3 milligrams on average were taken out of the mother liquor, dried using filter paper, crushed and then heated at a steady rate of 10 K min^{-1} in a vented pan for DSC analysis. Two identical 50 µl vented aluminium pans were utilized; one holds a sample, and the other is empty and serves as a reference. As a function of temperature or time, the changes brought about by the heating process and heat flow were noted for both the sample and the reference material. Melting, phase changes, and other thermal events can be observed on the DSC curve.

- ***Thermogravimetry (TGA)***

Chemical changes in the co-crystal/salt upon heating can be detected using thermogravimetric analysis. The weight of the sample is measured by the device in relation to time or temperature. A mass loss curve is the name given to a curve that is produced during the TGA analysis. Fractional weight and various stages of decomposition can be evaluated using TGA curves (Haines, 1995). Samples were removed from the mother liquor, dried and crushed before analysis in a Perkin-Elmer PC6-series TGA analyzer. Due to compound degradation, mass losses as a function of temperature measurement were observed when the samples were heated at a steady rate, usually 10 °C min^{-1}. The inert gas, nitrogen is used at a 20 mL min^{-1} flow rate. A measurement range of 30 to 300 °C was used.

2.2.4 Single Crystal X-Ray Diffraction

Single crystal X-ray diffraction is a non-destructive characterisation technique for the formation of new crystalline structures (Remenar, 2007). Single crystal X-Ray diffraction also provides information on unit cell dimensions, bond lengths and angles, and specifics of the crystalline material's site-ordering (Brown, 1973).

Single crystals of acceptable size and quality were chosen for single crystal X-ray diffraction to determine the crystal structure of each multicomponent crystal that was obtained. The data collections were carried out at the University of Cape Town using a Bruker APEX II diffractometer (Bruker, Karlsruhe, Germany). Graphite monochromated MoKα radiation (λ = 0.71073 Å) was used at 173 K. Crystal structure solutions and refinements were completed at the Cape Peninsula University of Technology.

The computer program used to solve the structures in the X-Seed interface (Barbour, ,2003) was SHELXS (Sheldrick, 2008). By feeding the programme XPREP (Bruker, 2004) with the gathered intensities and pre-established cell properties, the space group was ascertained. The structures were refined using SHELXL (Sheldrick, 2015). Mercury was used to generate the crystal structure images (Macrae et al., 2020).

2.2.5. Powder X-ray Diffraction

This technique can be used to differentiate the newly formed solid phases from the initial components, since each compound has a distinct diffraction line pattern because of its structural characteristics. The PXRD approach was utilized to identify new phases and compounds. PXRD can also provide unit cell dimensions (Karki, 2007). Samples were manually ground into powder and then put in an X-ray beam-path sample container. The instrument used to measure the PXRD patterns of the acquired products was a D2 PHASER Bruker diffractometer, which was equipped with Cu-Kα radiation (1.54184 Å). A scintillation counter, 1-dim LYNXEYE, and Xflash detector were used together with a voltage tube and current set at 30 kV and 10 mA max, respectively. Every sample was scanned in the range of 4 to 50° 2θ. The computed patterns (created from known structures using Mercury) and the PXRDs of the physical mixtures of the components were compared to the experimental powder patterns (Macrae et al., 2020).

2.2.6 Infrared (IR) Spectroscopy

A FTIR spectrum 1000 spectrometer was used in a dispersive mode with potassium bromide discs, which contain 250 mg of potassium bromide and 1 mg of the material, to do the Fourier transform infrared (FTIR) measurements. At a spectral resolution of 2 cm^{-1}, the resultant spectra were recorded within the range of 440 – 4400 cm^{-1}. The version of the IR instrument utilized was Spectrum V.5.3.1. Three distinct benefits of infrared spectroscopy are ease of use,

speed, and sensitivity. Furthermore, this method gives the ability to analyze samples in any state and provides a wealth of information about the spectral bands seen in compound FTIR spectra (Stuart,1996). The primary interaction that drives the infrared spectra is that of the atoms' vibrations within the molecule; the frequencies of these vibrations are indicative of the different functional groups.

2.2.7 Computing Packages

LAZY PULVERIX: LAZY PULVERIX's function is to use single crystal data to compute the theoretical powder X-ray diffraction pattern (Yvon, 1997).

POVRay: POVRay's function is to render images for structures.

XPREP: Bruker diffraction data processing. It is possible to configure SHELX input files and identify the space group.

PLATON: used in the computation of the molecular structure parameters (Spek, 2000)

ConQuest: used as the main application for looking for and obtaining data from the Cambridge Structural Database (Allen, 2002).

Mercury: software that makes it possible to examine and analyze crystal formations. It may be used to take a slice through a crystal in any direction, define and show Miller planes, and create packing diagrams. Additionally, it computes voids using the contact surface method or solvent accessible surface calculations (Macrae et al., 2020).

X-seed: a Windows program that generates high-quality molecular graphics images from crystal structure data and is intended to facilitate exploration, analysis, and editing of crystal structures (Barbour, 2020).

REFERENCES

Allen, F.H. 2002. The Cambridge Structural Database: A Quarter of a Million Crystal Structures and Rising. *Acta Cryst* Section B, 58, 380-388.

Barbour, L. J. 2003. X-Seed: Graphical interface for SHELX program. *J. Supramol. Chem.*, 1: 189-191.

Barbour, L. J. 2020. X-Seed 4: updates to a program for small-molecule supramolecular crystallography. *J. Appl. Cryst*. 53: 1141.

Brown, M.E. 2001. Introduction to Thermal Analysis: Techniques and Applications, Second Edition. 2nd ed. Norwell, Mass: Kluwer Academic Publishers.

Brown, P. J. and Forsyth. J. B. 1973.The crystal structure of solids. Edward Arnold Limited, London.

Macrae, C. F.; Sovago, I.; Cottrell, S. J.; Galek, P. T. A.; McCabe, P.; Pidcock, E.; Platings, M.; Shields, G. P.; Stevens, J. S.; Towler, M. and Wood, P. A., 2020. Mercury 4.0: from visualization to analysis, design and prediction. *J. Appl.* Cryst., 53: 226-235.

Diem, M.; Griffith, P. and Chalmers, J. 2008.Vibrational Spectroscopy for Medical Diagnosis, Wiley, New York.

Emadi, D; Whiting; L.V.; Nafisi, S.; Ghomashchi, R. 2005. Applications of thermal analysis in quality control of solidification processes, *J. Therm. Anal. Calorim.*, 81: 235–242.

Haines, P. J. 1995.Thermal Methods of Analysis. Blackie Academic & Professional, London.

Karki, S.; Fábián. L.; Friščić. T. and Jones, W. Powder X-ray Diffraction as an Emerging Method to Structurally Characterize Organic Solids, *Org. Lett*, 2007(9):3133-3136.

Karki, S.; Friščić, T.; Fabian, L. and Jones, W. 2010. New solid forms of artemisinin obtained through cocrystallisation. *CrystEngComm.*, *12*(12): 4038-4041.

Laudise, R. A. 1970. The Growth of Single Crystal. Solid State Physical Electronic Series INC, New Jersey.

Lesage-Meessen, L.; Delattre, M.; Haon, M.; Thibault, J.F.; Ceccaldi, B.C.; Brunerie, P.; Asther, M. 1996. A two-step bioconversion process for vanillin production from ferulic acid combining Aspergillus niger and Pycnoporus cinnabarinus. *J Biotechnol*. 50(2-3):107-13.

Naumann, D.; Helm, D. and Labischinski, H. 1991. Microbiological characterizations by FTIR spectroscopy, Nature, 351: 81–82.

Pov-Ray for Windows, Version 3. le Watcom. win32. The persistence of vision development team, © 1991-1999.

Remenar, J.F.; Peterson, M.L.; Stephens, P.W.; Zhang, Z.; Zimenkov, Y. and Hickey, M.B. 2007Celecoxib: Nicotinamide Dissociation Using Excipients to Capture the Cocrystal's Potential. Molecular Pharmacology, 4: 386-400.

Sheldrick, G. M. 2008.A short history of SHELX. *Acta Cryst.,* 64, 112–122.

Sheldrick, G. M. 2015.Crystal structure refinement with SHELXL., *Acta Cryst.,* C71, 3--8.

Spek, A.I. 2003. J. Appl. Cryst. 36: 7–13.

Stuart. B.; George. B. and McIntyre. P. 1996.Modern Infrared Spectroscopy, John Wiley & Sons, New York, USA.

XPREP, Data Preparation and Reciprocal Space Exploration, Version 5.1/NT© 1997, Bruker Analytical X-ray Systems.

Yvon, K., Jeitschko, W. & Parthe, E. J. 1997. LAZY PULVERIX, a computer program, for calculating X-ray and neutron diffraction powder patterns. *J. Appl. Cryst*, 10: 73-74.

CHAPTER 3: COCRYSTAL OF VANILLIC ACID WITH 4,4-BIPYRIDINE

3.1 Introduction

When crystalline materials made of neutral molecules are combined and the neutral molecules are kept together by noncovalent interactions, primarily hydrogen bonds, a cocrystal is produced (Bevill et al., 2014). This chapter describes the cocrystal formed with vanillic acid and 4,4-bipyridine. The compound was initially analyzed using FTIR spectroscopy due to its ease of usage, rapidity, and sensitivity (Stuart, 1996). Since the compounds are defined based on their melting points, the second stage of this investigation involved subjecting the same system to the DSC. Powder X-ray diffraction was then carried out since the structural features of each compound cause it to display a distinct PXRD pattern. Finally, single crystal X-Ray diffraction was performed. Figure 3.1 displays the chemical structures of the compounds used in this investigation.

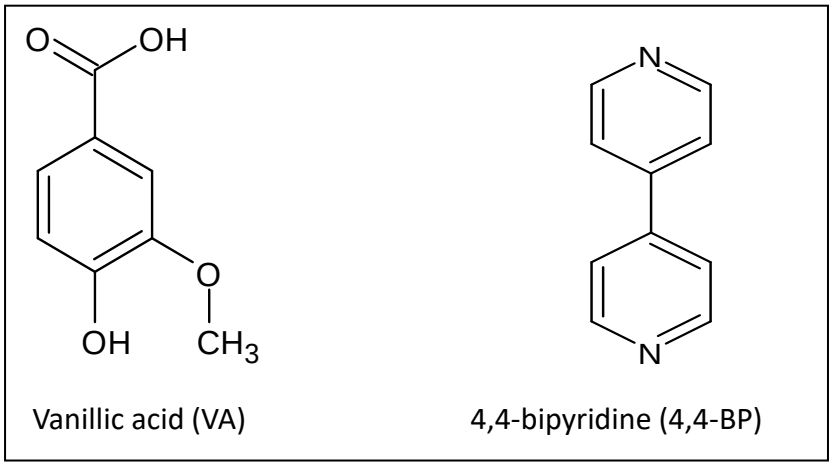

Figure 3.1: Chemical structures used in this study

3.2 Vanillic acid with 4,4-bipyridine (VA·4,4-BP)

In a 1:1 molar ratio (0.3 mmol), vanillic acid (VA) and 4,4 bipyridine formed a cocrystal, named as VA·4,4-BP. 2 ml of propan-2- ol was used to dissolve the mixture of 50 mg of vanillic acid and 46.3 mg of 4,4-BP in a vial on a hot plate. The mixture was gradually heated and stirred until the solids were dissolved completely. After a few days, the solution was allowed to evaporate and crystals in the shape of a block were produced. One molecule of VA and one molecule of 4,4-BP are present in the asymmetric unit (Figure 3.2). This structure was reported

by Angevine and Benedict, using methanol as solvent, however no additional analyses were done (Angevine & Benedict, 2022).

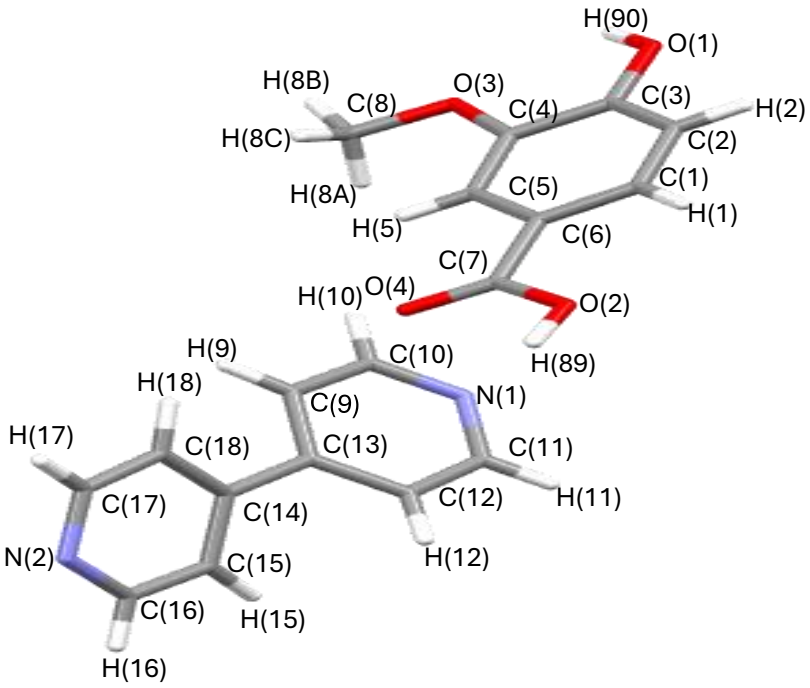

Figure 3.2: Asymmetric unit of the VA·4,4BP structure.

3.2.1 FTIR analysis

The infrared spectra of the cocrystal and starting materials are displayed in Figure 3.3. The spectra of VA·4,4-BP differs from that of the individual components. New interactions between the VA and 4.4-BP molecules in the cocrystal phase are indicated by the mobility and emergence of certain peaks. There are three noticeable changes: the C=O peak has shifted to the higher wave number, 1668 cm^{-1} in the cocrystal and the OH stretch which appears broader in the cocrystal structure has shifted to 3486 cm^{-1}. The nitrogens of the pyridine and the hydrogens of the vanillic acid interact through hydrogen bonds to cause this change. Table 3.1 displays the results of the FTIR analysis.

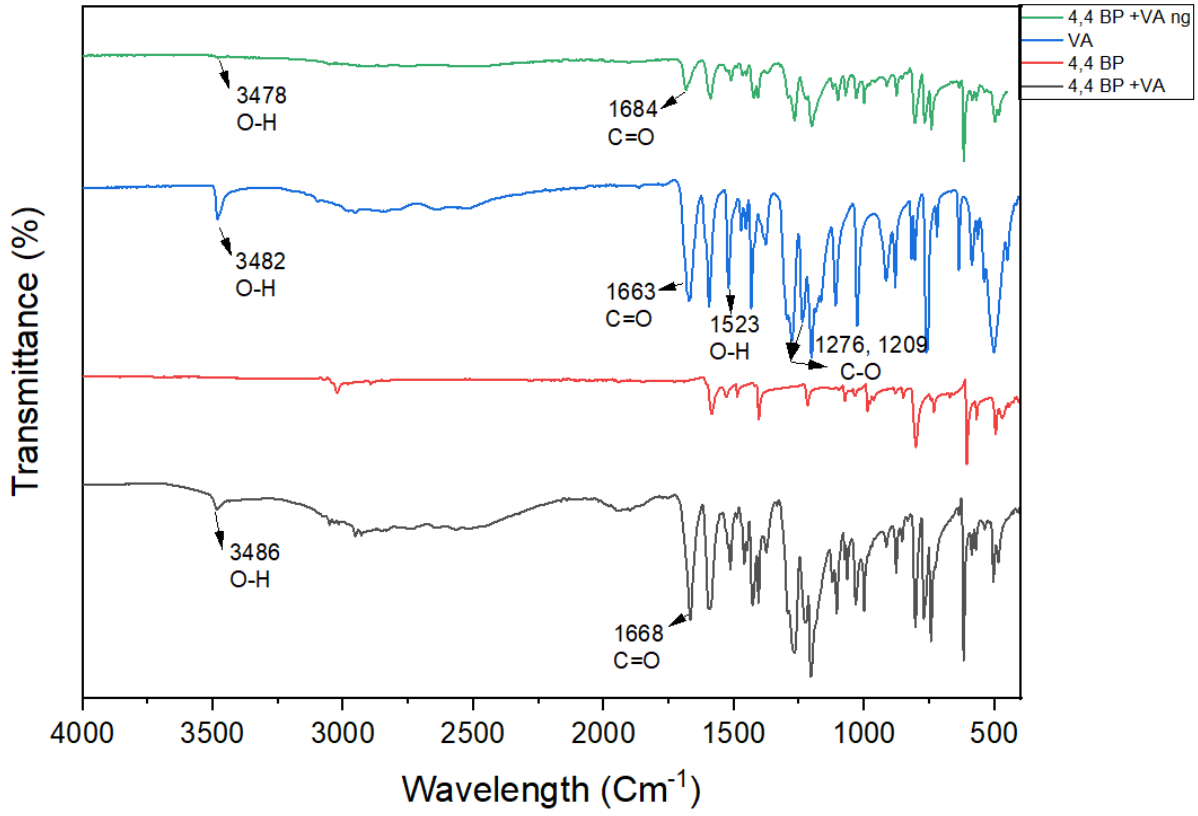

Figure 3.3: FTIR spectra of VA·4,4-BP Neat ground product, VA, 4,4-BP and VA·4,4-BP cocrystal.

Table 3.1: FTIR positions and assignments for the peaks in VA and VA.4,4-BP.

VA	**VA·4,4-BP**	**4,4-BP**	**Proposed assignment**
3482	3486	-	Free O-H stretch
1663	1668	-	C=O
1276, 1209	-	-	C-O stretch
-	1513	1583	C=N

3.2.2 Thermal analysis

The cocrystal's melting point, which is shown by a single broad endothermic peak on the VA·4,4-BP DSC curve, is 178.1 °C. The crystal melts between the two initial materials' melting points, VA (213.0 °C) and BIPY (113.5 °C) (Figure 3.4). Table 3.2 summarises the thermal analysis results.

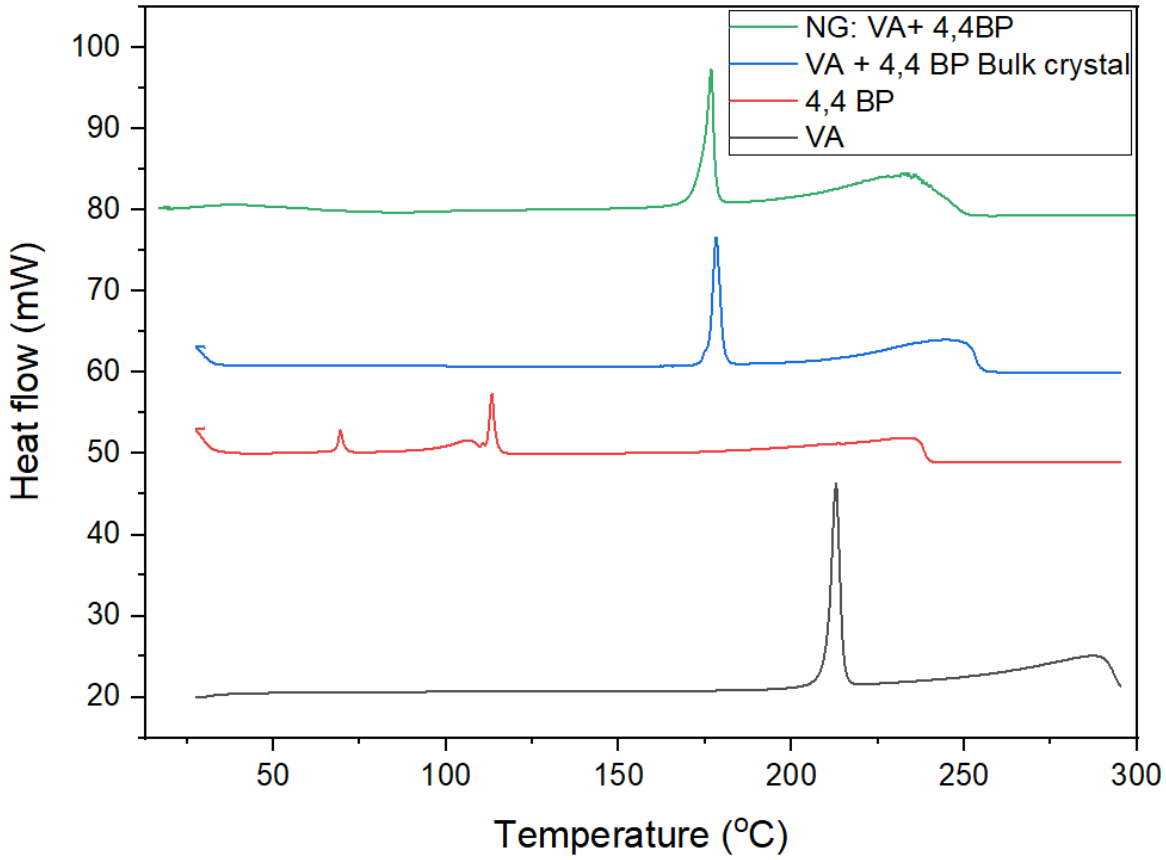

Figure 3.4: DSC curves of neat ground product of VA+ 4,4-BP (green), VA·4,4-BP Bulk crystal (blue), 4,4-BP (red) and VA (black).

Table 3.2: Thermal analysis data for VA·4,4-BP.

Compounds	**DSC $_{Endo}$ (T_{peak},°C)**
Vanillic acid	213.0
4,4-bipyridine	113.5
VA·4,4-BP	178.1
VA+4,4-BP Neat grinding	176.8

3.2.3 Powder X-ray Diffraction

To create the cocrystal, the solvent assisted grinding approach was employed. A few drops of propan-2-ol were added to a 1:1 VA·4,4-BP molar ratio and ground for 20 min. This experiment was repeated without the addition of solvent (neat grinding). The ground products' PXRD patterns were compared to those of the bulk crystal and the calculated pattern

from Mercury, Figure 3.5. The calculated and the bulk crystal patterns are in good agreement with the PXRD pattern of the solvent assisted ground product, however the PXRD pattern of the neat grinding experiment did not match any of the above-mentioned patterns, but it contains a few low-intensity peaks that corresponded to peaks in the estimated pattern and some peaks from the starting materials As a result, we can deduce that the powder from the neat grinding procedure contains unreacted starting materials.

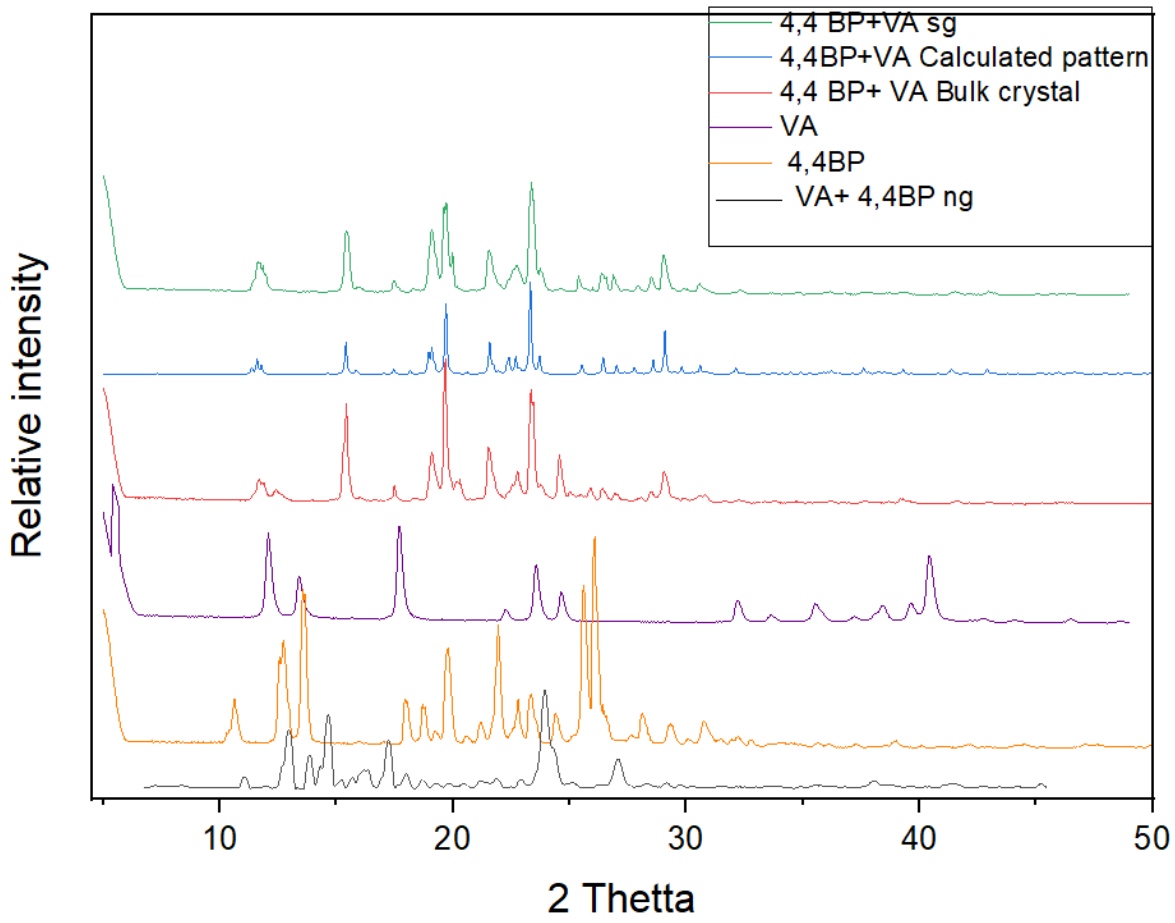

Figure 3.5: solvent assisted ground product (green), Calculated pattern of VA · 4,4-BP (blue), Bulk crystal (red), vanillic acid (purple), 4,4-BP (orange), ground product (black).

3.2.4 Crystal structure of VA·4,4-BP cocrystal

Following several days of gradual evaporation of 1:1 VA and 4,4-bipyridine (4,4-BP) in propan-2-ol at room temperature, colourless single crystals were produced. Using direct methods with SHELXS (Sheldrick, 2008), the structure was solved in the monoclinic space group $P2_1/c$ (Z = 4). According to the difference in pK_a between VA and 4,4-BP (5.25 – 4.16 = 1.09), which is in the region where cocrystals are most likely to form, no proton transfer was observed (Cruz-

Cabeza, 2012). The VA·4,4-BP cocrystal was thus produced. Table 3.3 summarizes the crystal data, this crystal data was the same as that obtained by Angevine and Benedict (Angevine & Benedict, 2022).

Table 3.3: Crystal data and refinement parameters of VA·4,4-BP.

Compound	**VA·4,4-BP**
Structural formula	$C_8H_8O_4 \cdot C_{10}H_8N_2$
VA·4,4BP	1:1
Molecular mass (g mol^{-1})	324.33
Data collection temperature (K)	173
Crystal system	Monoclinic
Space group	$P2_1/c$
a (Å)	13.460(3)
b (Å)	10.149(2)
c (Å)	12.848(3)
α (°)	90
β (°)	115.92(3)
γ (°)	90
Volume ($Å^3$)	1578.5(7)
Z	4
D_c, Calculated density (g cm^{-3})	1.365
Final R indices [I>2σ (I)]	R_1 = 0.0463 wR_1 = 0.1262
R indices (all data)	R_2 = 0.0525 wR_2 = 0.1313
Largest diff. peak and hole ($eÅ^{-3}$)	0.265; -0.380

O-H···N interactions define the structure (Figure 3.6). A vanillic acid molecule's oxygen (O2) is linked to one 4,4-bipyridine nitrogen atom (N1) through the hydrogen atom H89. The nitrogen (N2) of the 4,4-bipyridine is linked to the second hydrogen (H90) of the vanillic acid molecule (Table 3.4). The O-H···N hydrogen bonding between the VA and 4,4-BP molecules form

$C_2^2(17)$ chains. These interactions between VA and 4,4-BP molecules in the VA·4,4-BP cocrystal phase were described by Angevine and Benedict (Angevine & Benedict, 2022).

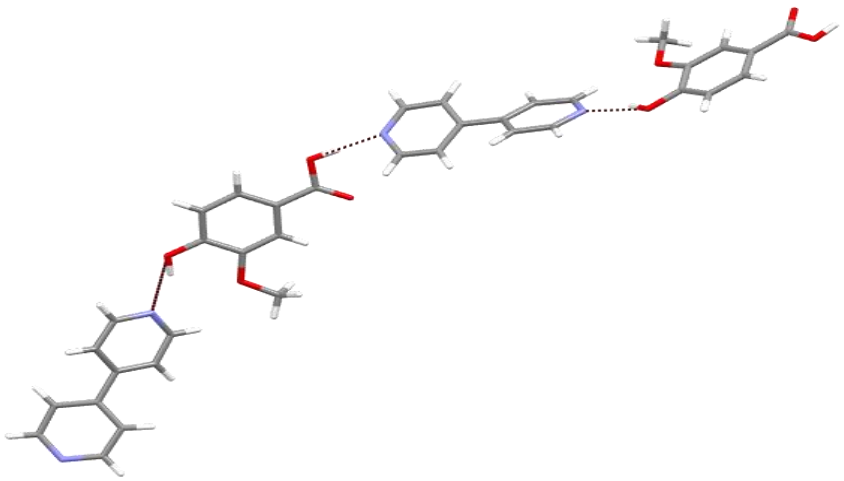

Figure 3.6: Hydrogen bonds of VA·4,4-BP cocrystal.

Table 3.4: Geometrical data for hydrogen bond of VA·4,4-BP.

D-H···A	**D···A (Å)**	**D-H (Å)**	**H···A (Å)**	**D-H···A (°)**	**Symmetry operations**
O2-H89…N1	2.7169(17)	0.91(2)	1.83(2)	162(2)	x, y, z
O1-H90…N2	2.7146(17)	0.87(3)	1.91(3)	143(2)	$x-1, \frac{3}{2}-y, \frac{1}{2}+z$

A few weak interactions also contribute to the structure's stabilization: π-π stacking interactions between adjacent vanillic acid molecules with a distance between centroids of 4.0113(9) Å. There are C12-H12-π (d = 3.4843(8) Å) and C17-H17-π (d = 3.6248(8) Å) interactions involving 4,4-bipyridine molecules. The hydrogen-bonded units are arranged as continuous zigzag patterns parallel to the b axis (Figure 3.7).

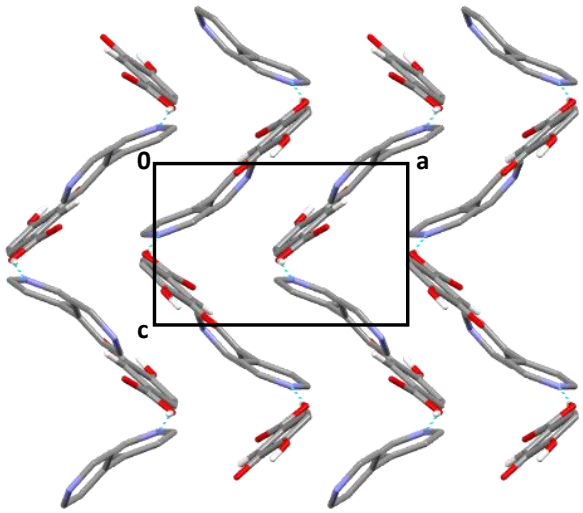

Figure 3.7: Packing diagram of VA·4,4-BP.

3.3 Summary

The pK_a rule indicated that the new solid form was a cocrystal. Using single crystal X-ray diffraction, the VA·4,4-BP cocrystal was characterized. The crystal structure shows clearly that this is a co-crystal which was confirmed by the C-O distances since no proton transfer was observed (C-O bond distance of d(C7-O2) = 1.3295 (18) Å and C=O distance of d(C7-O4) = 1.2092 (18) Å). The structure was solved in the monoclinic space group $P2_1/c$ with Z = 4. The shift of the OH and C=O bands in the cocrystal originating from the starting material is also evidently seen using FTIR spectroscopy. The melting point of the VA·4,4-BP cocrystal, which was discovered to be greater than that of 4,4-BP and lower than that of VA, was determined to be 178.1°C. PXRD analysis verified that the same compound was produced during the synthesis of the cocrystal employing the solvent assisted grinding process. An O-H···N supramolecular heterosynthon was present in the cocrystal, and this resulted in the formation of $C_2^2(17)$ chains.

REFERENCES

Angevine, D. J. and Benedict, J. B. 2022. The co-crystal structure of 4-hydroxy-3-methoxybenzoic acid – 4,4′-bipyridine, $C_8H_8O_4 \cdot C_{10}H_8N_2$. *Z. Kristallogr. - New Cryst. Struct*. 237: 397–398.

Chettri, A.; Subba, A.; Singh, G. P. and Bag, P. P. 2023. Pharmaceutical co-crystals: A green way to enhance drug stability and solubility for improved therapeutic efficacy. *J Pharm. Pharmacol*. 1–12.

Cruz-Cabeza, A., 2012. Acid–base crystalline complexes and the pK_a rule. *CrystEngComm*, 14: 6362-6365.

Bevill, M. J.; Vlahova, P. I. and Smit, J. P. 2014. Polymorphic cocrystals of nutraceutical compound p-coumaric acid with nicotinamide: Characterization, relative solid-state stability, and conversion to alternate stoichiometries. *Cryst. Growth & Des.*, 14(3): 1438-1448.

Sheldrick, G. A. 2008. short history of SHELX. *Acta Cryst*, 64: 112–122.

Yvon, K.; Jeitschko, W. and Parthe, E. J. 1997. *LAZY PULVERIX*, a computer program, for calculating X-ray and neutron diffraction powder patterns. *J. Appl. Cryst,* 10: 73-74.

CHAPTER 4: SALTS OF VANILLIC ACID

4.1 Introduction

When two molecules (base and acid) with a pK_a difference of at least two units are combined, a salt is produced (Serajuddin, 2002). Vanillic acid was chosen because it contains three different functional groups that can create hydrogen bonds: -COOH, -OH, and -OCH_3. (Lesage-Meessen, 1996). In this study vanillic acid formed salts with 4-dimethylaminopyridine (4DMAP), 2-amino-5-methylpyridine (A25MP), and 2-amino-6-methylpyridine (A26MP). The focus is on the preparation and characterisation of the vanillic (VA) acid salts formed. The study's chemical structures are depicted in Figure 4.1.

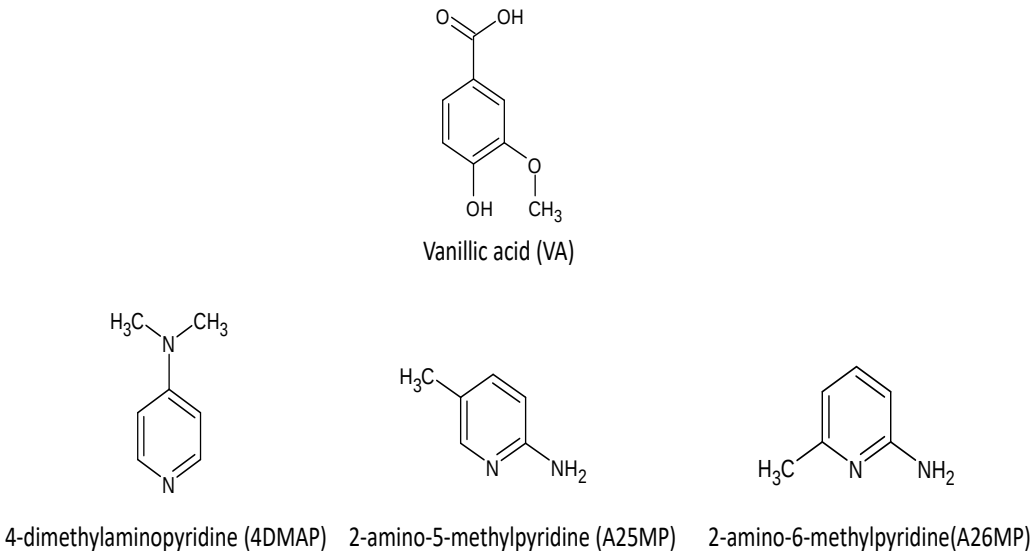

Figure 4.1: Chemical structures used in this study.

4.2 Vanillic acid and 4-dimethylaminopyridine (VA^-)($4DMAP^+$)

4-Dimethylaminopyridine (4DMAP) is a white solid compound derivative of pyridine. Because of the resonance stabilization provided by the -$N(CH_3)_2$ substituent, it is more basic than pyridine (Berry et al., 2007). A 1:1 molar ratio (0.3 mmol) of vanillic acid (50mg) and 4-dimethylaminopyridine (36mg) was dissolved in 2 ml of propan-2-ol on a hot plate while stirring. Crystals were formed a few days after the solution was left to evaporate at room temperature. Figure 4.2 depicts the asymmetric unit of (VA^-)($4DMAP^+$).

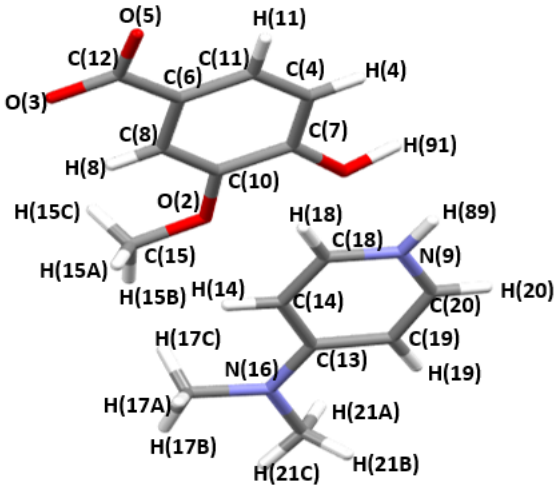

Figure 4.2: Asymmetric unit of the $(VA^{-})(4DMAP^{+})$ structure with all the hydrogen atoms shown for numbering clarity.

4.2.1 FTIR spectroscopy

The FTIR spectrum of $(VA^{-})(4DMAP^{+})$ (Figure 4.3) displays peaks at 3095 cm^{-1} and 1644 cm^{-1}, which represents the OH and COO^{-} stretches, respectively. The OH stretch of the salt appears as a broad band compared to the narrow band of vanillic acid, these changes show that the nitrogens of the pyridine and the hydrogens of the vanillic acid interact through hydrogen bonds, resulting in the creation of the salt. Table 4.1 lists the FTIR positions and assignments.

Table 4.1: FTIR positions and assignments of peaks for VA, $(VA^{-})(4DMAP^{+})$ and 4DMAP.

VA	**$(VA^{-})(4DMAP^{+})$**	**4DMAP**	**Proposed assignment**
3482	3095	-	Free O-H stretch
1523	-	-	O-H
1663	-	-	C=O
-	1644	-	COO^{-}
1276, 1209	-	-	C-O stretch
-	1011	1092	C=N

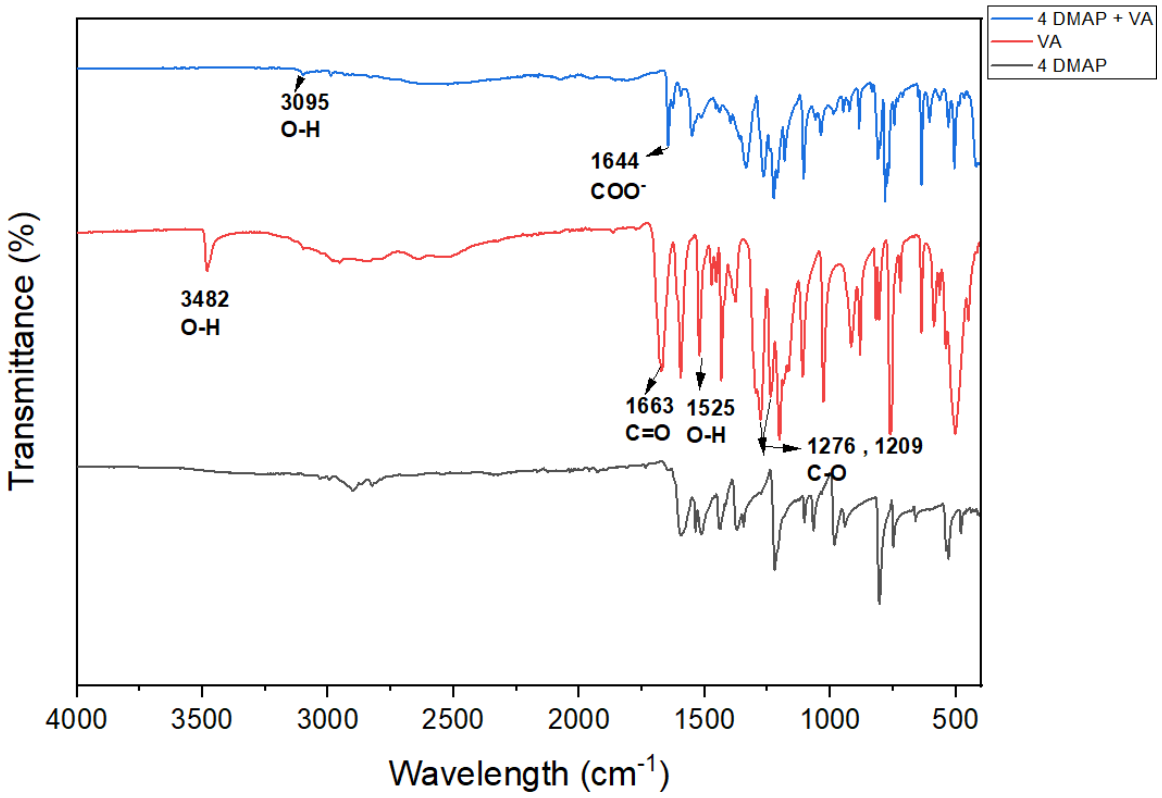

Figure 4.3: FTIR spectra of (VA^-)($4DMAP^+$) (blue), VA (red) and 4DMAP (black).

4.2.2 Thermal analysis

The salt produced, as shown in Figure 4.4, has an endotherm on its DSC curve that differs from the melts of VA or 4DMAP. The melting point of the salt is between those of the starting materials (Table 4.2). The second broad endotherm in the DSC is due to the decomposition of the salt.

Table 4.2: Thermal analysis data of VA, 4DMAP and (VA^-)($4DMAP^+$).

Compounds	**DSC $_{Endo}$(°C)**
Vanillic acid	213
4-Dimethylaminopyridine	116
(VA^-)($4DMAP^+$)	163

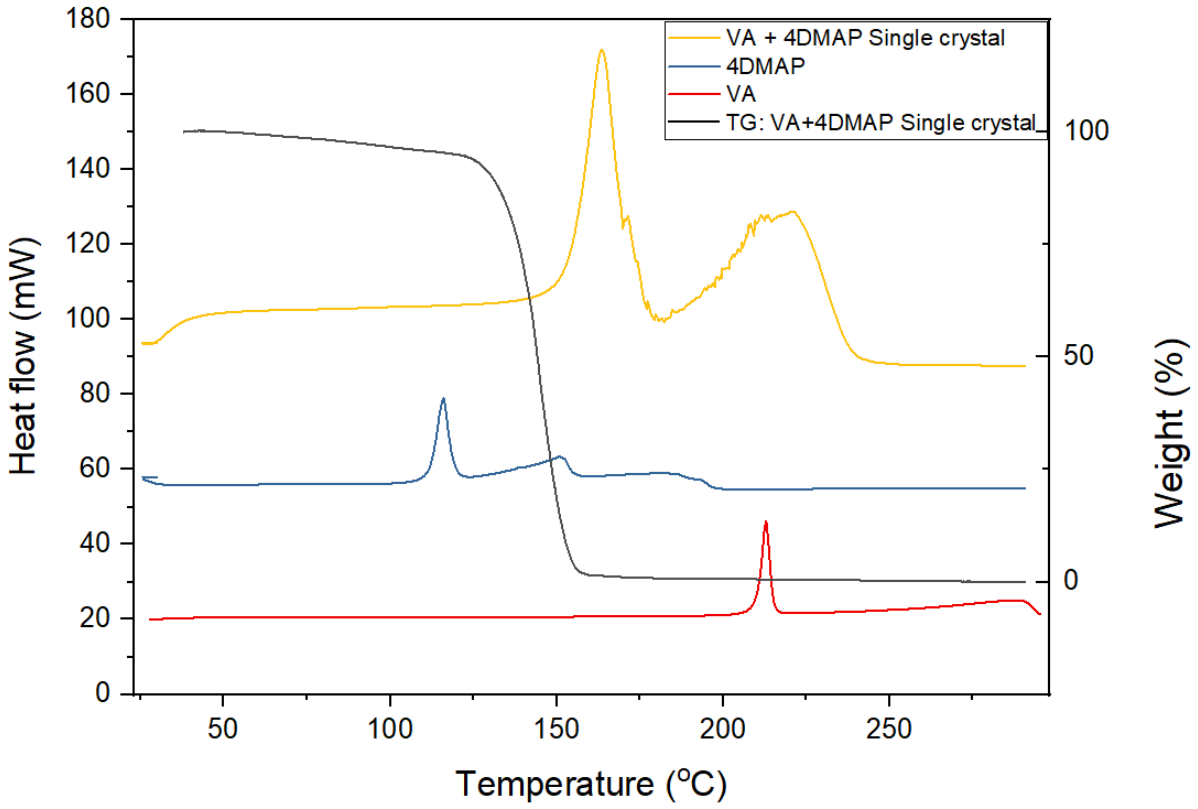

Figure 4.4: DSC curves of (VA^-)($4DMAP^+$) (yellow), 4DMAP (blue) and VA (red) and TG curve of (VA^-)($4DMAP^+$) (black).

4.2.3 Powder X-ray diffraction

A 1:1 molar ratio VA and 4DMAP were finely ground and the resultant powder displayed a PXRD pattern with some peaks from the 4DMAP pattern, but it mainly resembled the single crystal pattern (Figure 4.5). This shows that the ground product has partially converted. The PXRD pattern of the solvent-assisted grinding in propan-2-ol also indicated partial reaction. The PXRD of the bulk crystal agreed well with the calculated pattern obtained from Mercury.

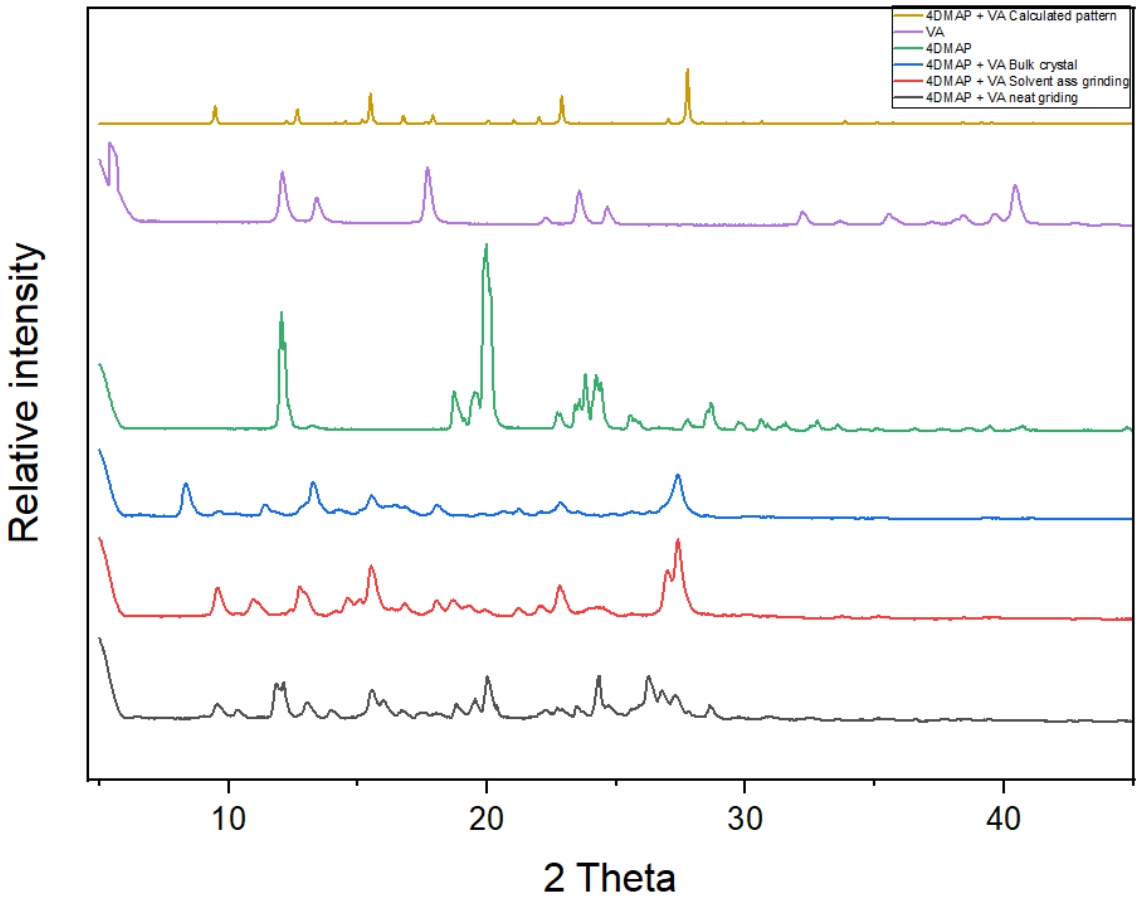

Figure 4.5: PXRD patterns of (VA^-)($4DMAP^+$) (gold), VA (purple), 4DMAP (green), bulk crystal (blue), solvent assisted ground product (red) and neat ground product (black).

4.2.4 Structure determination

In a 1:1 ratio, VA and 4DMAP formed colourless crystals that resembled blocks. Using direct methods, the structure was solved in the monoclinic space group $P2_1/n$. The crystal data parameters are displayed in Table 4.3 below.

Table 4.3: Crystal data and refinement parameters of the (VA^-)($4DMAP^+$) salt.

Compound	**(VA^-)($4DMAP^+$)**
Structural formula	$(C_8H_7O_4)^-(C_7H_{11}N_2)^+$
Ratio	1:1
M_r ($gmol^{-1}$)	290.31

Temperature (K)	173
Crystal system	Monoclinic
Space group	$P2_1/n$
a (Å)	8.1530(16)
b (Å)	13.975(3)
c (Å)	12.637(3)
α (°)	90
β (°)	97.45(3)
γ (°)	90
Volume ($Å^3$)	1427.7(5)
Z	4
D_c, Calcd density ($g\ cm^{-3}$)	1.351
Final R indices [I>2 σ (I)]	R_1= 0.0448 wR_1= 0.1107
R indices (all data)	R_2 = 0.0652 wR_2 = 0.1247
Largest diff. peak and hole ($eÅ^{-3}$)	0.301; -0.297

A heterosynthon (N_{pyr}^{+}-H···COO^{-}) was created when the carboxylic acid group of the VA was deprotonated to the pyridine's nitrogen in 4DMAP. Additionally, the phenol OH generates O-H···O hydrogen bonds with the VA carboxylate group. As illustrated in Figure 4.6, the O1 of a vanillate anion is connected to the O3 of another VA by H1, and one 4-dimethylaminopyridinium nitrogen atom, designated N9, is connected to the oxygen (O5) of a vanillate anion via the hydrogen H90. Table 4.4 provides a summary of the hydrogen bond geometry data.

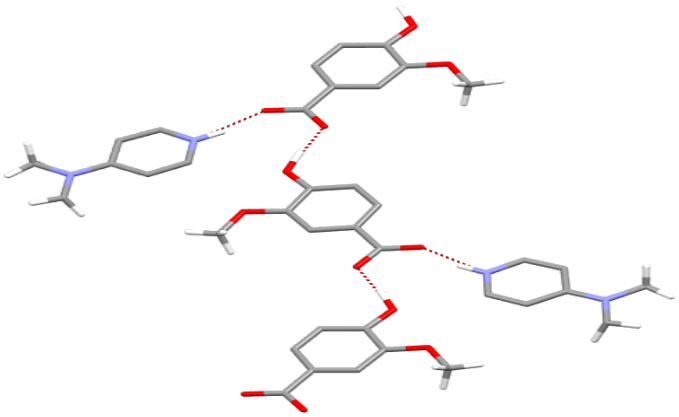

Figure 4.6: Hydrogen bond of (VA^-)($4DMAP^+$) salt with some hydrogen atoms omitted for clarity.

Table 4.4: Geometrical data for hydrogen bonds of (VA^-)($4DMAP^+$).

Compound	**D-H···A**	**D···A (Å)**	**D-H (Å)**	**H···A (Å)**	**D-H···A (°)**	**Symmetry operations**
(VA^-)($4DMAP^+$)	N9-H90…O5	2.6700(15)	0.93(2)	1.76(2)	164.0(17)	$x+\frac{1}{2},\frac{3}{2}-y,\frac{1}{2}+z$
	O1-H1…O3	2.5066(14)	0.958(15)	1.551(15)	175(2)	$x-1,\frac{3}{2}-y,\frac{1}{2}+z$

The structure is also stabilized by weak interactions (π- π stacking) which were observed between the vanillic acid aromatic ring (C4-C11) and the six membered ring of the 4-dimethylaminopyridine (N9-C13) with a Cg-Cg (distance between ring centroids) of 3.5545(8) Å. The packing diagram shows $C_1^1(8)$ chains parallel to the b axis, Figure 4.7.

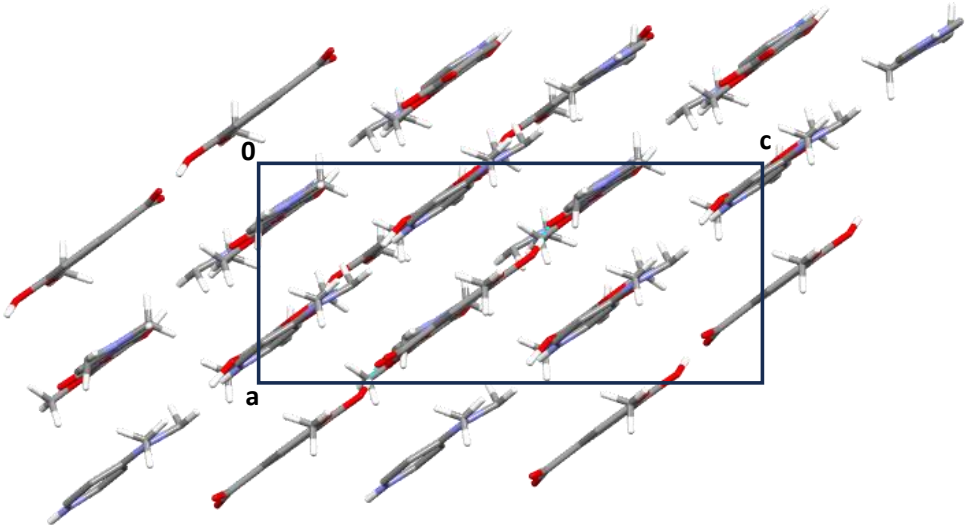

Figure 4.7: Packing diagram of (VA^-)(4DMAP$^+$) along [010] with hydrogen atoms omitted.

4.3 Vanillic acid and 2-amino-5-methylpyridine ($2VA^-$)(2A25MP$^+$)

0.3 mmol of both VA (50mg) and A25MP (32mg) were dissolved in 2 ml of propan-2-ol with heating on a hot plate to yield the ($2VA^-$)(2A25MP$^+$) salt. Crystals were formed after two days by allowing the solution to evaporate under ambient conditions. The resulting salt has two VA anions and two A25MP cations in the asymmetric unit (Figure 4.8).

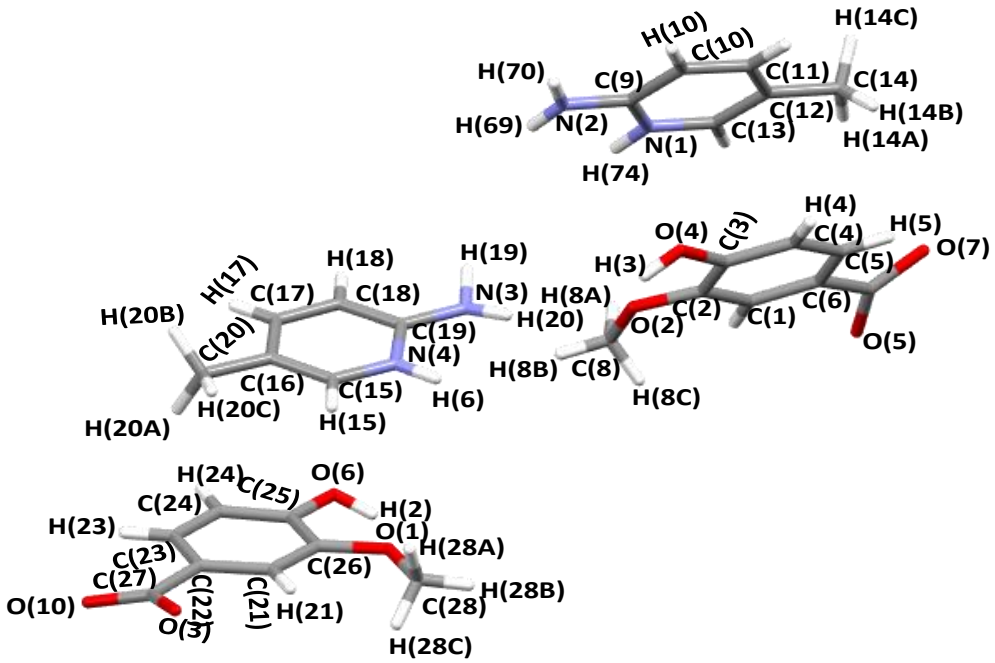

Figure 4.8: Asymmetric unit of the ($2VA^-$)(2A25MP$^+$) structure with all the hydrogen atoms shown for numbering clarity.

4.3.1 FTIR spectroscopy

Figure 4.9 shows the FTIR spectra of the starting compounds as well as the new compound obtained. Infrared spectroscopy makes it possible to probe the vibrational modes of a molecule and to associate the vibration frequencies with functional groups. For A25MP alone, the N-H stretch is identified by two bands around 3453 cm^{-1} and 3416 cm^{-1}. The band at 1624 cm^{-1} corresponds to the NH_2 bend. For VA, a peak linked to the stretching of the C=O double bond of the carboxylic acid is observed at 1663 cm^{-1}, as well as a peak at 3482 cm^{-1} corresponding to the stretching of the free OH bond.

The salt $(2VA^-)(2A25MP^+)$ presents an FTIR spectrum significantly different from those of the starting compounds alone. The movement and appearance of certain peaks indicate the formation of new interactions between VA and A25MP in the crystalline phase. Three major shifts are visible: the NH_2 bend peak have moved toward higher wave number (1640 cm^{-1}). This movement signals the contraction of the bond between nitrogen in the NH_2 group and the oxygen of the carboxylic acid. Likewise, the peak at 1674 cm^{-1} corresponds to the COO^- stretch and occurs at a higher wavenumber than the C=O of VA. This modification is due to an elongation of the C=O bond in the formation of the salt. The presence of a broad band at 3290 cm^{-1} is also visible. This band is the result of hydrogen bonding of the free NH_2 groups. The FTIR positions and assignments are given in Table 4.5.

Table 4.5: FTIR positions and assignments of peaks in VA, A25MP and $(2VA^-)(2A25MP^+)$.

VA	**A25MP**	**$(2VA^-)(2A25MP^+)$**	**Proposed assignments**
3482	-	2932	Free O-H stretch
1523	-	1347	O-H
1663	-		C=O
-	-	1674	COO^-
1276, 1209			C-O stretch
-	3453, 3416	3290	N-H stretch
	1624	1640	NH_2 bend

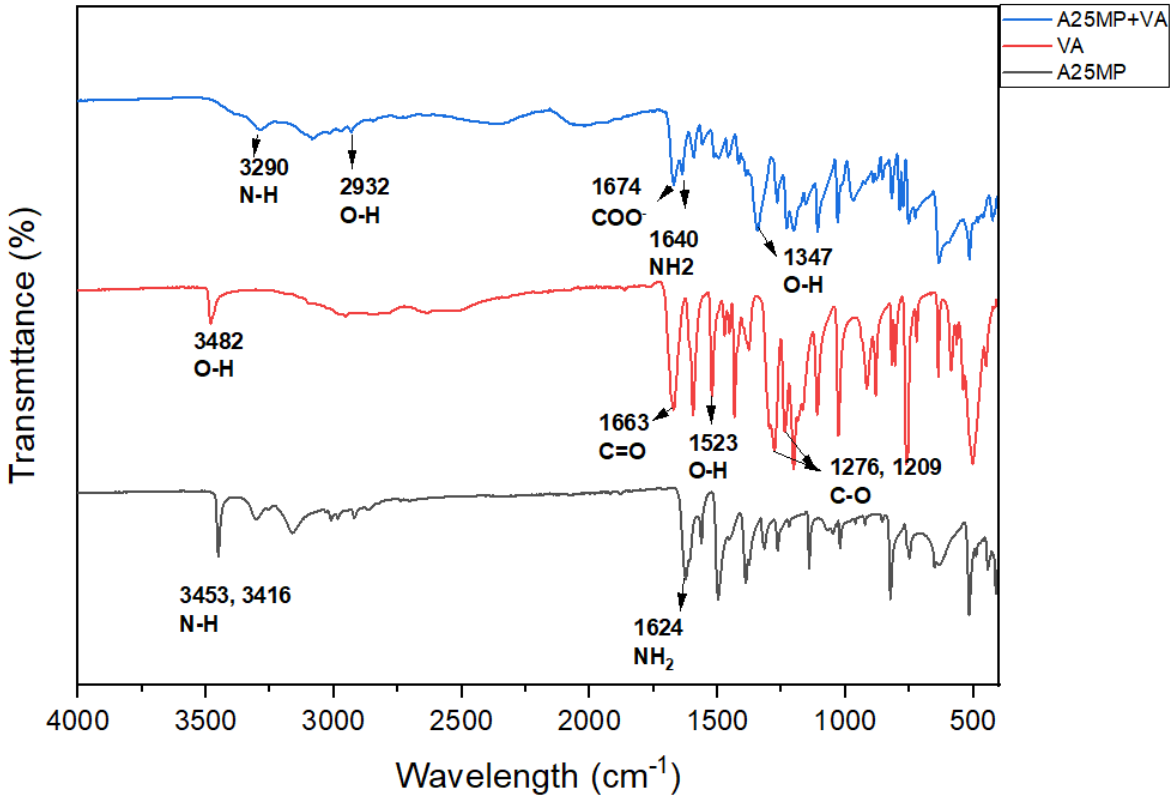

Figure 4.9: FTIR spectra of ($2VA^{-}$)($2A25MP^{+}$) (blue), VA (red) and A25MP (black).

4.3.2 Thermal analysis

The melting point of the salt was found to be in-between the two starting components. Thermal analysis data and curves are shown in Table 4.6 and Figure 4.10 respectively.

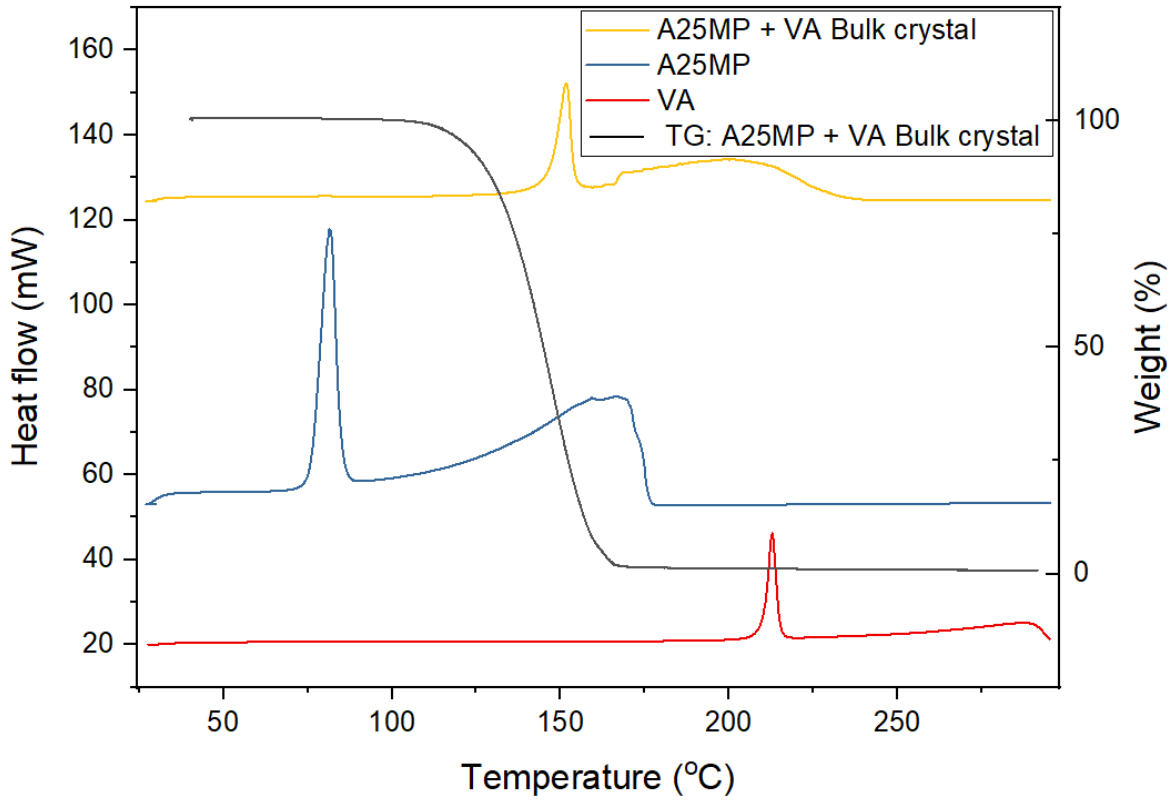

Figure 4.10: DSC curves of VA (red), A25MP (blue) , $(2VA^{-})(2A25MP^{+})$ (yellow) and TG of $(2VA^{-})(2A25MP^{+})$(black).

Table 4.6: Thermal analysis data of VA, A25MP and $(2VA^{-})(2A25MP^{+})$.

Compounds	**DSC $_{Endo}$(°C)**
Vanillic acid	213
2-amino-5-methylpyridine	81
$(2VA^{-})(2A25MP^{+})$	152

4.3.3 Powder X-ray Diffraction

The calculated pattern from Mercury and the PXRD pattern of the bulk crystal show good agreement. Neither the bulk crystal PXRD pattern nor the calculated pattern derived from Mercury matched the PXRD pattern of the ground products in any of the two approaches. Both resulted in physical mixtures of the starting materials. Figure 4.11 illustrates the PXRD patterns for the various types of experiments.

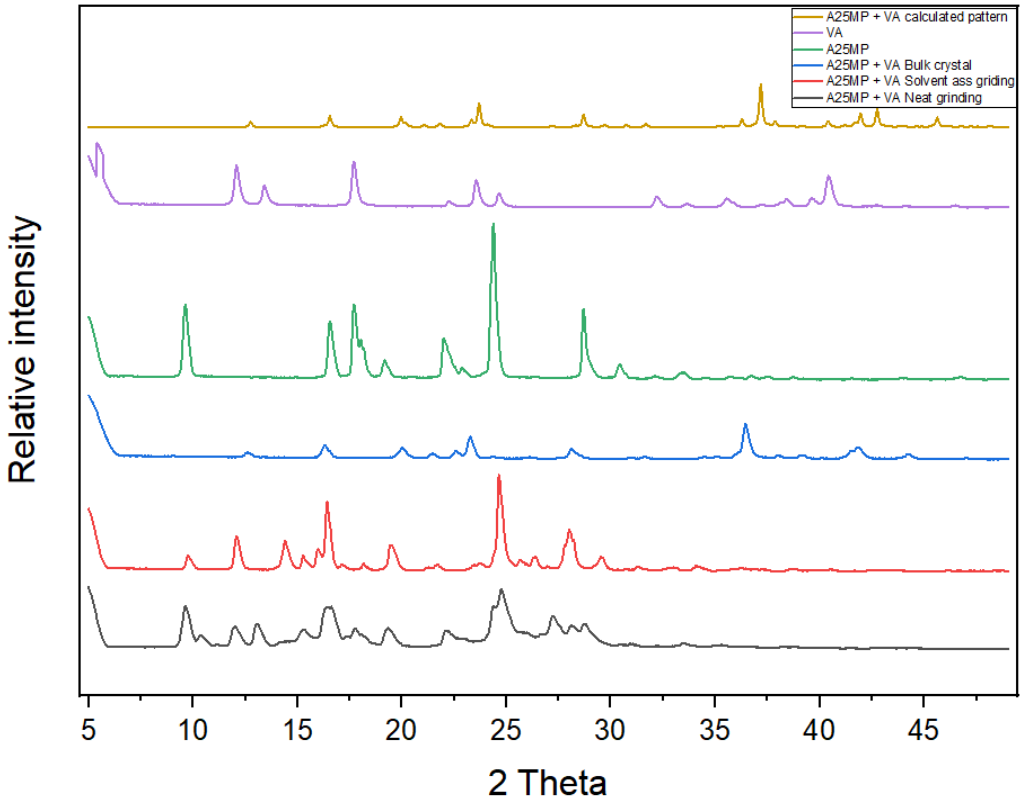

Figure 4.11: PXRD patterns of $(2VA^{-})(2A25MP^{+})$ (gold), VA (purple), A25MP (green), bulk crystal (blue), solvent assisted ground product (red) and ground product (black).

4.3.4 Structure Determination

VA with A25MP formed colourless block-like crystals with a 2:2 ratio of VA:A25MP. The structure was solved in the monoclinic space group $P2_1$, using direct methods. Table 4.7 below illustrates the crystal data parameters.

Table 4.7: Crystal data and refinement parameters of ($2VA^{-}$)($2A25MP^{+}$) salt.

Compound	**($2VA^{-}$)($2A25MP^{+}$)**
Structural formula	$(2C_8\,H_8\,O_4)^{-}\,(2C_6\,H_8\,N_2)^{+}$
Ratio	2:2
M_r ($gmol^{-1}$)	552.57
Temperature (K)	173
Crystal system	Monoclinic
Space group	$P2_1$
a (Å)	7.7104(15)
b (Å)	11.501(2)
c (Å)	14.939(3)
α (°)	90
β (°)	102.81(3)
γ (°)	90
Volume ($Å^3$)	1291.8(5)
Z	2
D_c, Calcd density (gcm^{-3})	1.421
Final R indices [I>2 σ (I)]	R_1= 0.0303 wR_1= 0.0769
R indices (all data)	R_2= 0.0327 wR_2= 0.0785
Largest diff. peak and hole ($eÅ^{-3}$)	0.648; -0.275

Four hydrogen bonds involving nitrogen are present in the salt of ($2VA^{-}$)($2A25MP^{+}$): two $N_{pyr}{}^{+}$-H···O^{-} (pyridinium carboxylate synthon) and two N-H···O^{-} (amine carboxylate synthon). Moderate O-H···O hydrogen bonds are also present. A summary of the hydrogen bond data is provided in Table 4.8. The 2-aminopyridinium carboxylate heterosynthon forms $R_2^2(8)$ rings. The VA^{-} anions are linked to $A25MP^{+}$ cations via N-H···O hydrogen bonding forming $C_2^2(11)$, and $C_1^2(7)$ chains, and VA^{-} anions are linked together via O-H···O hydrogen bonding forming $C_1^1(8)$ chains. The hydrogen bonding is shown in Figure 4.12. There are π···π stacking interactions between A25MP and VA rings with d(Cg-Cg) = 3.7111(7) Å and there are also π···π

stacking interactions between another A25MP ring and a VA ring with d(Cg-Cg) = 3.9878(8) Å. The packing diagram shows zig-zag chains parallel to the c axis, Figure 4.13.

Table 4.8: Geometrical data for hydrogen bond of ($2VA^{-}$)($2A25MP^{+}$).

Compound	**D-H···A**	**D···A (Å)**	**D-H (Å)**	**H···A (Å)**	**D-H···A (°)**	**Symmetry operations**
($2VA^{-}$)($2A25MP^{+}$)	N3-H19…O3	2.968(2)	0.90(3)	2.03(3)	172(2)	$1-x,\frac{1}{2}+y,-z$
	N2-H69…O3	2.919(2)	0.85(3)	2.09(3)	167(3)	$1-x,\frac{1}{2}+y,-z$
	N1-H74…O10	2.632(2)	0.92(3)	1.72(3)	170(3)	$1-x,\frac{1}{2}+y,-z$
	O4-H3…O5	2.7364(19)	0.84(3)	1.93(3)	161(3)	$1-x,y-\frac{1}{2},1-z$
	N3-H20…O5	2.890(2)	0.93(3)	2.01(3)	158(3)	$1-x,y-\frac{1}{2},1-z$
	O6-H2…O3	2.760(2)	0.81(3)	1.98(3)	159(3)	$2-x,\frac{1}{2}+y,-z$

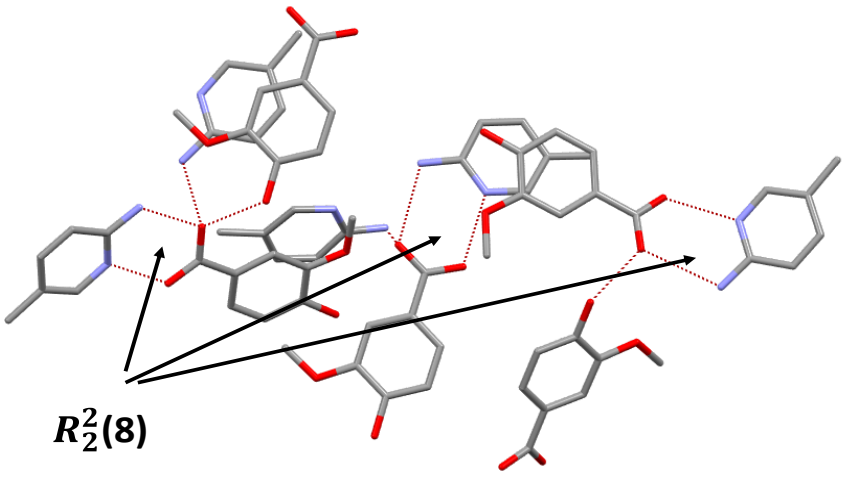

Figure 4.12: Hydrogen bond of 2(VA^{-})·2($2A5MP^{+}$) salt with some hydrogen atoms omitted for clarity.

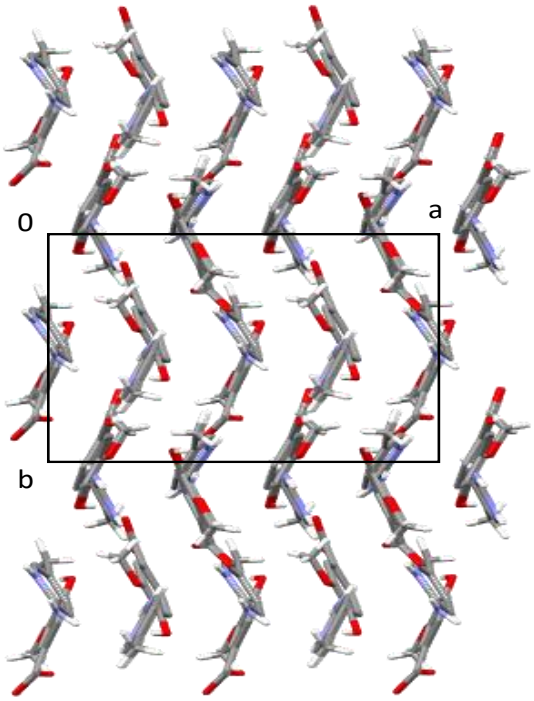

Figure 4.13: Packing diagram of ($2VA^{-}$)($2A25MP^{+}$) along [001] with hydrogen atoms omitted.

4.4 Vanillic acid and 2-amino-6-methylpyridine (VA^{-})($A26MP^{+}$)

A 1:1 molar ratio of VA (0.3 mmol, 50 mg) and A26MP (32 mg) was dissolved in 2 ml of ethanol using a hot plate. After two days of allowing the solution to evaporate at ambient temperature, crystals were formed. The acid-base combination resulted in a salt due to the ΔpK_a (pK_a (base) - pK_a (acid) = 7.6 - 4.16 = 3.44). Figure 4.14 depicts the asymmetric unit of the (VA^{-})($A26MP^{+}$) salt, which includes one molecule each of VA and A26MP.

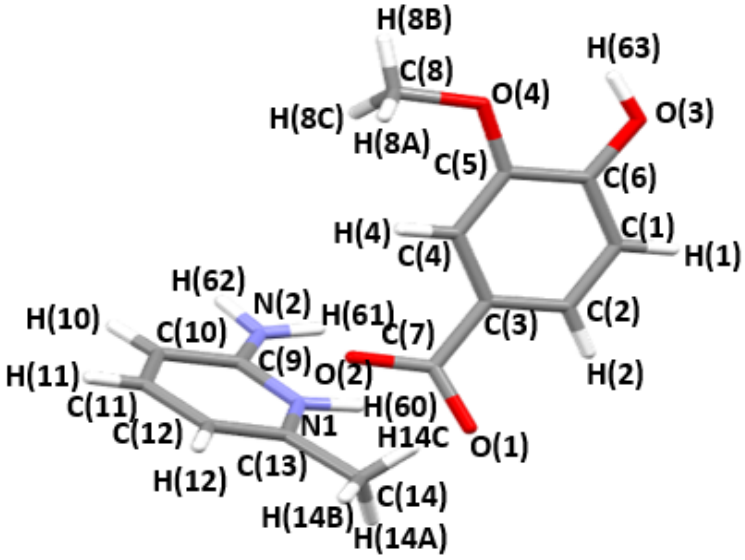

Figure 4.14: Numbering scheme of the asymmetric unit of (VA⁻)(A26MP⁺).

4.4.1 FTIR spectroscopy

The resulting salt (VA⁻)(A26MP⁺) has a distinct FTIR spectrum compared to the components alone. The shifting and development of specific peaks reflect the formation of new contacts between VA and A26MP molecules in the crystalline phase. Three shifts are visible: the narrow band at 3458 cm^{-1} in the A26MP becomes a broad band at 3521 cm^{-1} in the salt. This band results from a hydrogen bond interaction between the N-H of A26MP and the OH group of VA (Figure 4.15). The NH_2 peak at 1625 cm^{-1} in the A26MP has moved to the higher wave number (1639 cm^{-1}) in the salt. This displacement indicates a constriction of the bonds between the nitrogen of the NH_2 group and the oxygen of the carboxylic acid. Similarly, the signal at 1681 cm^{-1} corresponds to COO^- derived from vanillic acid. This change results from the elongation of the C=O in the formation of the salt. The FTIR positions and assignments are shown in Table 4.9.

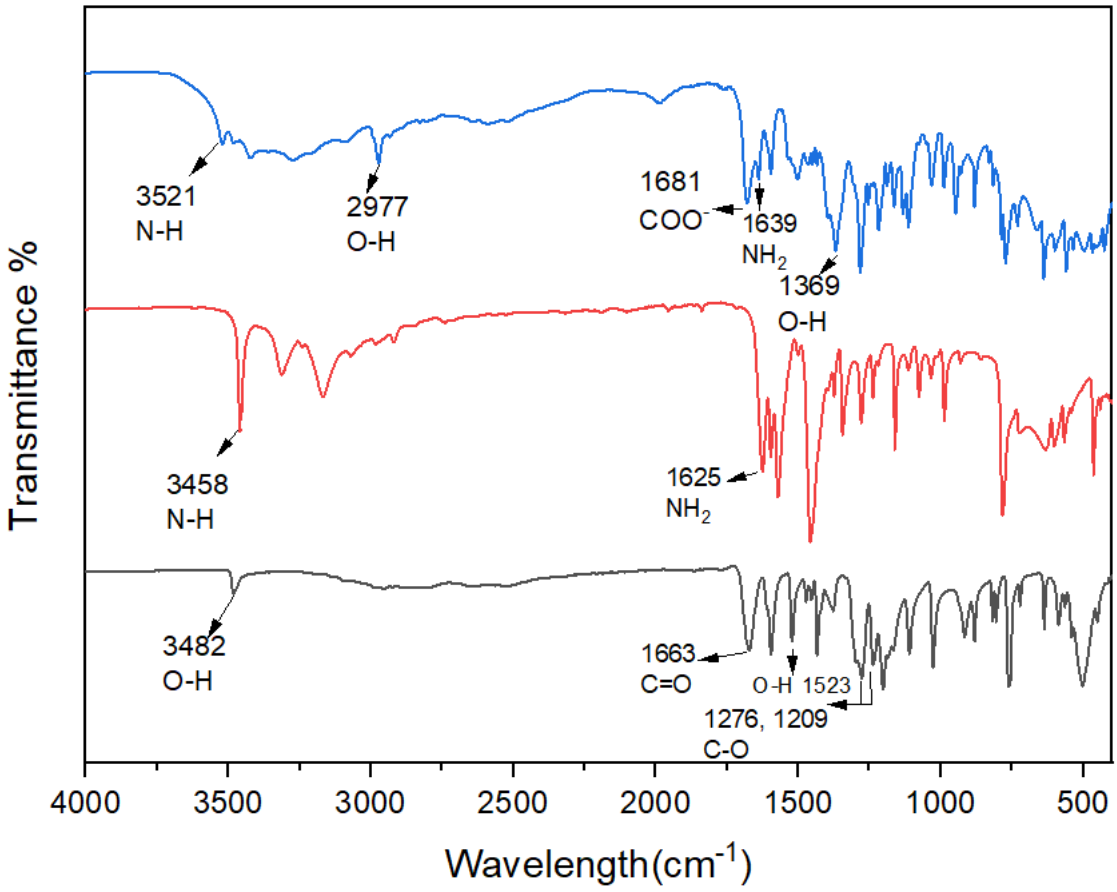

Figure 4.15: FTIR spectrums of (VA⁻)(A26MP⁺) (blue), A26MP (red) and VA (black).

Table 4.9: FTIR positions and assignments of peaks in VA, A26MP and (VA⁻)(A26MP⁺).

VA	**A26MP**	**(VA⁻)(A26MP⁺)**	**Proposed assignments**
3482	-	2977	Free O-H stretch
1523	-	1369	O-H
1663	-		C=O
-	-	1681	COO^-
1276, 1209		1281, 1217	C-O stretch
-	3458	3521	N-H stretch
	1625	1639	NH_2 bend

4.4.2 Thermal analysis

DSC was used to characterize A26MP and VA, as well as their salt. The $(VA^-)(A26MP^+)$ salt has an endothermic peak at 91.4 °C that corresponds to the loss of 0.15 A26MP. This endothermic peak coincides with an experimental mass loss of 5.72% in the TGA curve. The second endothermic peak at 169 °C is due to the melt of the intermediate (Figure 4.16). The thermal analysis data are summarized in Table 4.10.

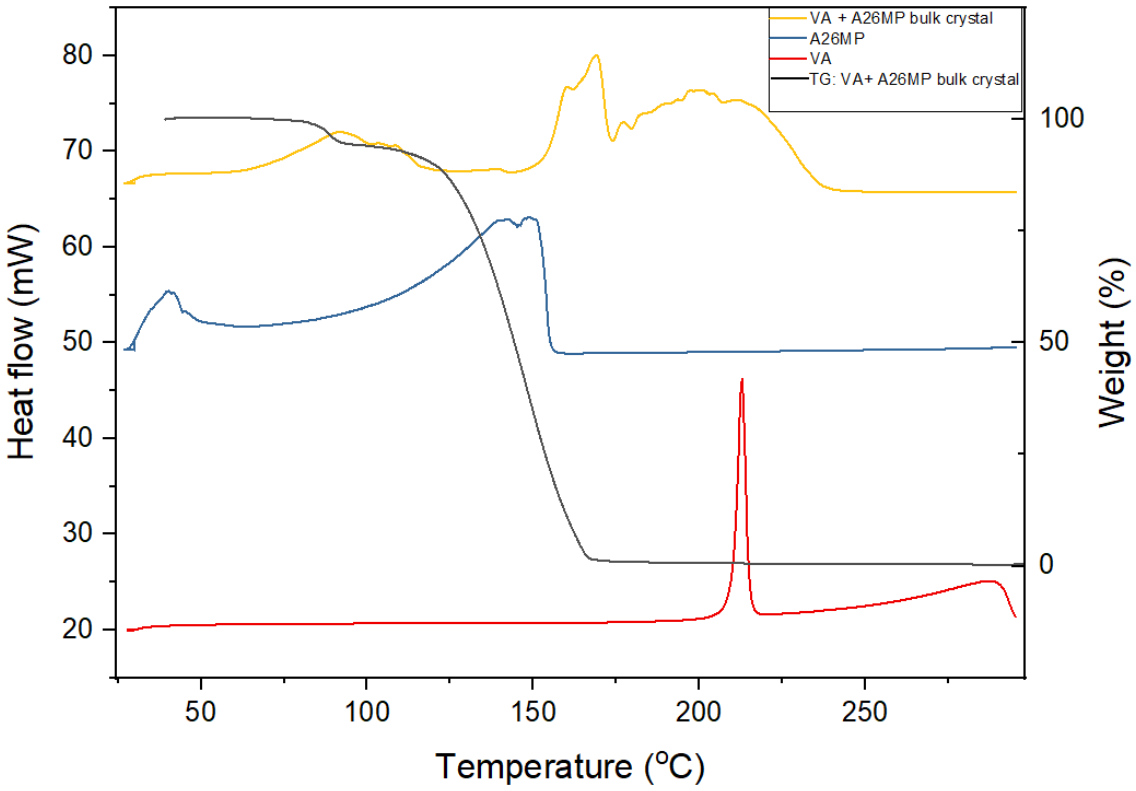

Figure 4.16:TG:$(VA^-)(A26MP^+)$ (black), DSC curves of VA (red), A26MP (blue) and $(VA^-)(A26MP^+)$ (yellow).

Table 4.10: Thermal analysis data of $(VA^-)(A26MP^+)$.

Compounds	**DSC $_{Endo}$(°C)**
Vanillic acid	213
2-amino-6-methylpyridine	40
$(VA^-)(A26MP^+)$	91,4 ; 169

4.4.3 Powder X-ray Diffraction

A mortar was filled with an equimolar mixture of VA and A26MP, which was ground for 20 minutes. The same procedure was followed with a few drops of solvent (ethanol), and both products were examined using PXRD. The PXRD patterns of the ground products were compared with the calculated pattern. The ground PXRD pattern shared many similarities with the calculated and the bulk crystal patterns and a few peaks of A26MP, indicating that the reaction was incomplete. Some similar peaks were identified in the solvent-assisted ground product pattern, as well as in the bulk crystal and calculated patterns, indicating that a partial reaction occurred (Figure 4.17).

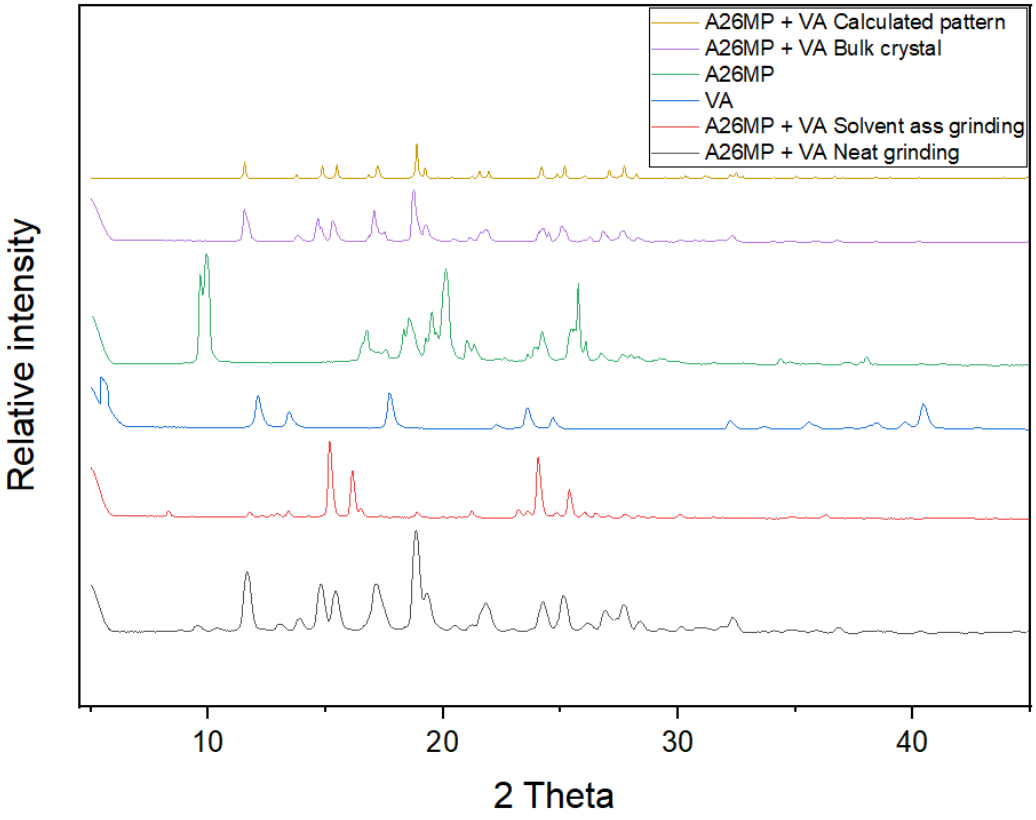

Figure 4.17: calculated patterns of (VA⁻)(A26MP⁺) (gold), VA (purple), ground product (green), A26MP (blue), bulk crystal (red), solvent assisted ground product (black).

4.4.4 Structure determination

The salt of $(VA^-)(A26MP^+)$ produced colourless block-like crystals with a 1:1 stoichiometry and was solved in the orthorhombic space group *P*bca. The structure was refined to $R_1 = 0.0393$ and $wR_2 = 0.0959$ ([I>2 σ (I)]. The crystal data for $(VA^-)(A26MP^+)$ is shown in Table 4.11.

Table 4.11: Crystal data and refinement parameters of $(VA^-)(A26MP^+)$.

Compound	**$(VA^-)(A26MP^+)$**
Structural formula	$(C_8\ H_8\ O_4)^-(C_6\ H_8\ N_2)^+$
Ratio	1:1
M_r ($gmol^{-1}$)	276.29
temperature (K)	173
Crystal system	orthorhombic
Space group	*P*bca
a (Å)	11.458(2)
b (Å)	11.917(2)
c (Å)	20.499(4)
α (°)	90
β (°)	90
γ (°)	90
Volume ($Å^3$)	2799.1(10)
Z	8
D_c, Calcd density (gcm^{-3})	1.311
Final R indices [I>2 σ (I)]	$R_1 = 0.0393$ $wR_1 = 0.0895$
R indices (all data)	$R_2 = 0.0513$ $wR_2 = 0.0959$
Largest diff. peak and hole ($eÅ^{-3}$)	0.320; -0.222

The 2-amino-6-pyridinium carboxylate heterosynthon forms $R_2^2(8)$ rings (Figure 4.18). The VA^- anions are coupled to $A26MP^+$ cations via N-H···O hydrogen bonding, generating $C_2^1(6)$, $C_2^2(6)$, and $C_1^1(8)$ chains that create a wave-like pattern in the packing diagram (Figure 4.19).

There are π···π stacking interactions between pyridine rings with d(Cg-Cg) = 3.798 Å and a CH-π stacking interaction with a distance of 3.774 Å between H8B and a vanillic acid ring. Geometrical data for the hydrogen bonds of $(VA^-)(A26MP^+)$ are presented in Table 4.12.

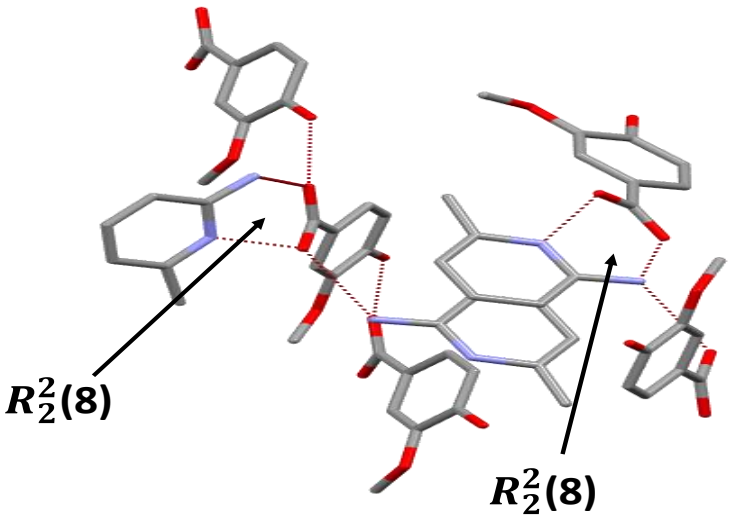

Figure 4.18: Hydrogen bond of $(VA^-)(A26MP^+)$ salt with some hydrogen atoms omitted for clarity.

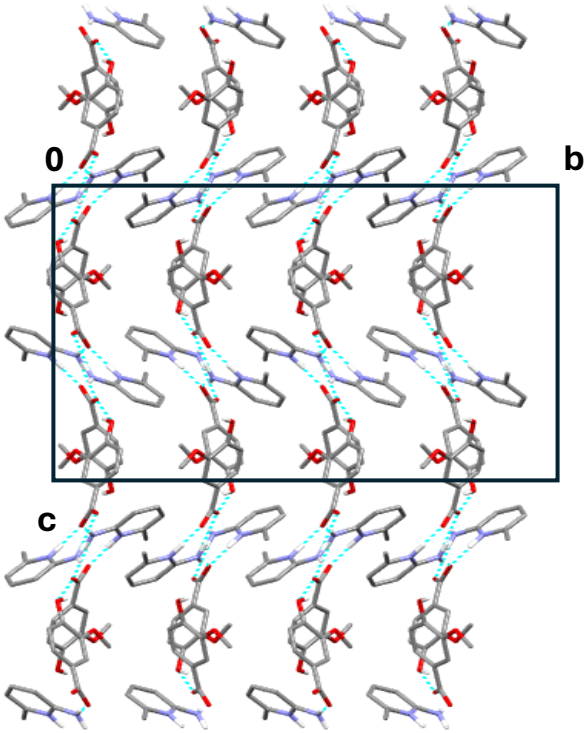

Figure 4.19: Packing diagram of (VA⁻)(A26MP⁺) along [100] with some hydrogen atoms omitted.

Table 4.12: Geometrical data for hydrogen bonds of (VA⁻)(A26MP⁺).

Compound	D-H···A	D···A (Å)	D-H (Å)	H···A (Å)	D-H···A (°)	Symmetry operations
(VA⁻)(A26MP⁺)	N1-H61…O1	2.8754(15)	0.907(19)	1.976(19)	171.0(16)	$1-x, 1-y, 1-z$
	N2-H60…O2	2.6544(15)	0.99(2)	1.67(2)	176.7(19)	$\frac{1}{2}-x, \frac{1}{2}+y, z$
	O3-H63…O1	2.6435(2)	0.90(2)	1.83(2)	149.9(19)	$\frac{1}{2}-x, \frac{1}{2}+y,$

4.5 Summary

As predicted by the pK_a rule, VA formed salts with 4DMAP, A25MP and A26MP. All the nitrogen atoms contained in the structures were involved in hydrogen bonding and displayed heterosynthons with the vanillic acid OH and COO^- groups except for A26MP which formed a

heterosynthon with the COO^- group of vanillic acid only with the nitrogen of the pyridine ring. The salts of VA with 4DMAP and A25MP were solved in the monoclinic crystal system in the space group $P2_1/n$ and $P2_1$ respectively and for VA and A26MP the structure was solved in the orthorhombic *P*bca space group. All three structures display $C_1^1(8)$ chains in their packing diagrams. For the $(2VA^-)(2A25MP^+)$ and $(VA^-)(A26MP^+)$ salts' structures, the 2-amino-6-pyridinium carboxylate heterosynthon formed $R_2^2(8)$ rings. The new compounds formed have been confirmed by the DSC analysis with different melting points from the starting materials for each salt formed. The thermal stability trend as determined by the DSC melting points is $(VA^-)(A26MP^+)$> $(2VA^-)(2A25MP^+)$ > $(VA^-)(4DAMP^+)$..

REFERENCES

Berry, D.J.; Digiovanna, C.V.; Metrick, S.S. and Murugan, R. 2001. Catalysis by 4-dialkylaminopyridines. *Arkivoc: 201–226*.

Lesage-Meessen, L.; Delattre, M.; Haon, M.; Thibault, J.F.; Ceccaldi, B.C.; Brunerie, P. and Asther, M. 1996. A two-step bioconversion process for vanillin production from ferulic acid combining Aspergillus niger and Pycnoporus cinnabarinus. *J. Biotechnol.* 50: 107–113.

Serajuddin, A.T.; Pudipeddi, M.; Stahl, P.H. and Wermuth, C.G. editors. 2002. Handbook of pharmaceutical salts. Weinheim: Wiley-VCH; p. 138.

Sheldrick, G. M. 1997. Program for the Refinement of Crystal Structures from Diffraction Data. University of Göttingen, Göttingen, Germany.

Yvon, K., Jeitschko, W. and Parthe, E. J., 1997. LAZY PULVERIX, a computer program, for calculating X-ray and neutron diffraction powder patterns. *J. Appl. Cryst*, 10: 73-74.

CHAPTER 5: SALT HYDRATES OF VANILLIC ACID

5.1 Introduction

Organic salts are crystalline solids composed of ionizable molecules bound together by hydrogen bonds (Cruz-Cabeza, 2012). When a salt is linked to one or a particular number of water molecules, it becomes a hydrated salt or hydrate, hence hydrates are a type of multi-component crystal with applications in crystal engineering and medicinal science. Water molecules are easily incorporated into crystal lattices due to their modest size and diverse hydrogen bonding properties (Gillon et al., 2003). Hydrates may be the preferred active pharmaceutical ingredients crystal form due to their higher hydration stability compared to anhydrates (Clarke, 2010). This chapter concentrates on the synthesis and characterization of the salt hydrates of 4-aminopyridine and 2-aminopyridine with vanillic acid.

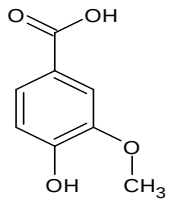

Vanillic acid

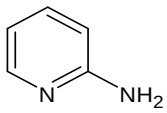

2-aminopyridine

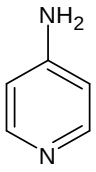

4-aminopyridine

Figure 5.1: Chemical structures used in this study.

5.2 Vanillic acid and 2-aminopyridine (3(VA^-)3($A2MP^+$)·H_2O)

2-aminopyridine, or $H_2NC_5H_4N$, is one of the three isomers of aminopyridines, a colourless solid used in medication synthesis (Chorlton et al., 2007).
The salt hydrate was formed by dissolving 50 mg of vanillic acid and 29 mg of 2-aminopyridine in 2 ml of ethanol in a 1:1 molar ratio (0.3 mmol) and allowing the solution to evaporate at room temperature. A single crystal from the bulk was analyzed using single crystal X-ray diffraction, and the structure was successfully solved in the monoclinic space group $P2_1/n$, with three vanillate anions, three 2-aminopyridinium cations and one molecule of water in the asymmetric unit (Figure 5.2).

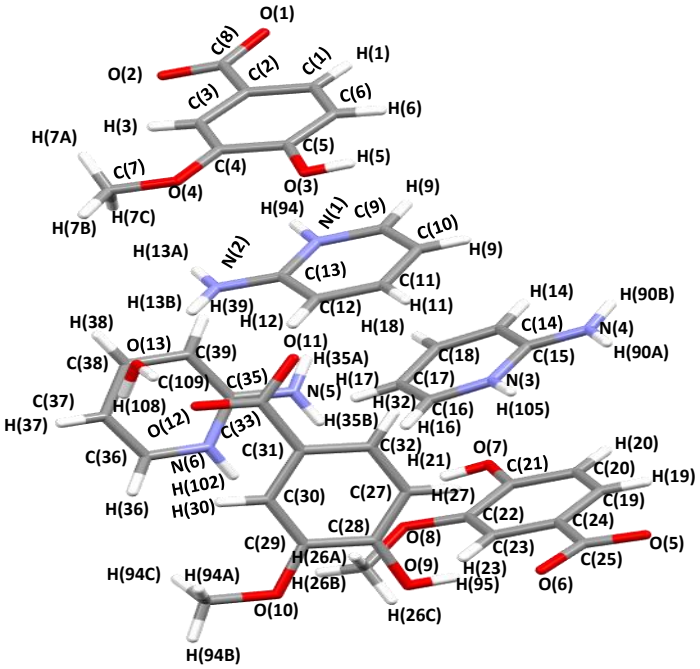

Figure 5.2: Asymmetric unit of the 3(VA⁻)3(A2MP⁺)·H_2O structure with all the hydrogen atoms shown for numbering clarity.

5.2.1 FTIR spectroscopy

Figure 5.3 depicts the FTIR spectrum of the salt hydrate 3(VA⁻)3(A2MP⁺)·H_2O. Salt formation was confirmed by the shift and establishment of new connections between the initial components. The shift of the NH_2 peak from 1623 cm^{-1} to 1592 cm^{-1} shows the establishment of a hydrogen bond between the nitrogen of the NH_2 group and the oxygen of the carboxylic acid. This new bond creation is the consequence of the shift in the C=O (1663 cm^{-1}) vibration band which correspond to COO^- (1493 cm^{-1}) in the salt hydrate. FTIR positions and assignments of peaks in VA, A2MP and 3(VA⁻)3(A2MP⁺)·H_2O are presented in Table 5.1.

Table 5.1: FTIR positions and assignments of peaks in VA, A2MP and 3(VA⁻)3(A2MP⁺)·H₂O.

VA	A2MP	3(VA⁻)3(A2MP⁺)·H₂O	Proposed assignments
3482	-	3358	O-H stretch
1523	-	1387	O-H
1663	-		C=O
-	-	1493	COO^-
1276, 1209			C-O stretch
-	3444, 3291	3554, 3486	N-H stretch
	1623	1592	NH_2 bend

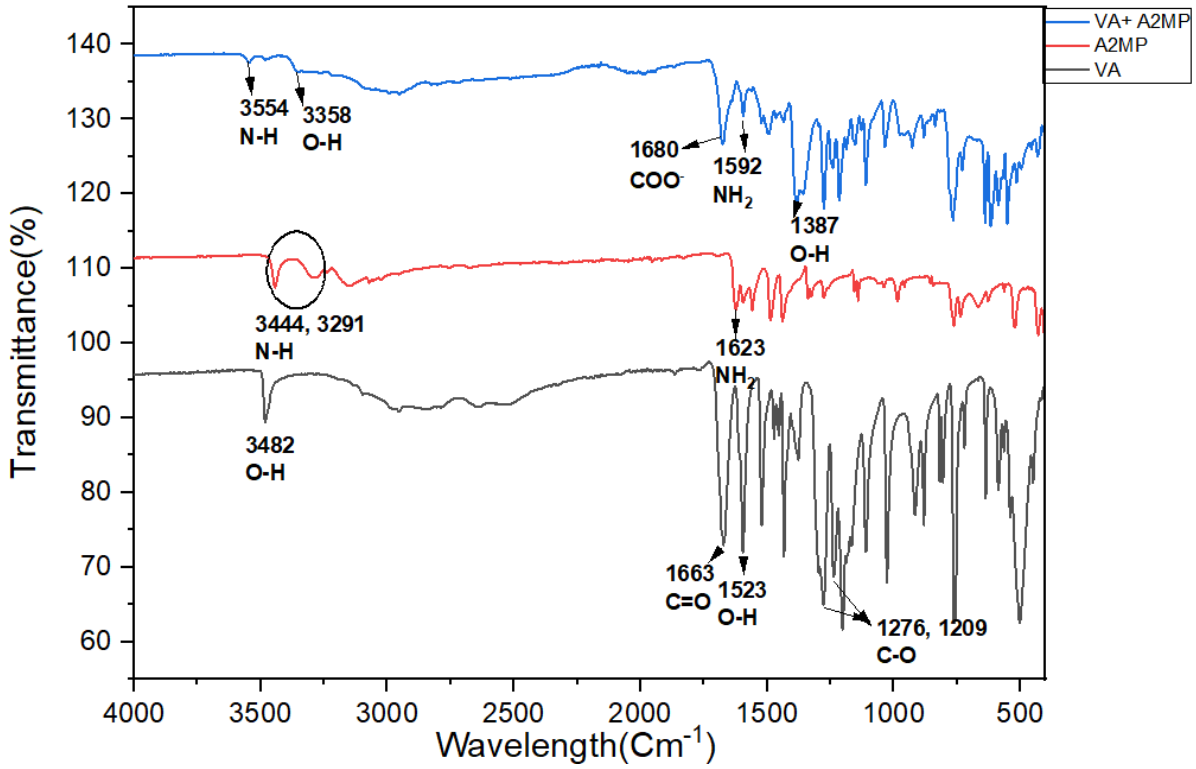

Figure 5.3: FTIR spectra of 3(VA⁻)3(A2MP⁺)·H₂O (blue), A2MP (red) and VA (black).

5.2.2 Thermal analysis

The 3(VA⁻)3(A2MP⁺)·H₂O salt hydrate has a melting point of 117 °C, which is between the two starting components as given in Table 5.2. The TG curve shows two mass loss steps. The first

step of 3.26 % corresponds to the loss of one water molecule (calc 2.23 %) and is also associated with the melt of the salt hydrate. The second step is due to the decomposition of the salt. Thermal analysis curves of $3(VA^{-})3(A2MP^{+})\cdot H_2O$, vanillic acid and 2-aminopyridine are illustrated in Figure 5.4.

Table 5.2: Thermal analysis data for $3(VA^{-})3(A2MP^{+})\cdot H_2O$.

Compounds	**Vanillic acid**	**2-aminopyridine**	**$3(VA^{-})3(A2MP^{+})\cdot H_2O$**
DSC Endo1(T_{onset},°C)	213	61.6	117
DSC Endo2(T_{onset},°C)			197.7
TG calc % mass loss			2.23
TG exp % mass loss	-	-	3.26
VA: A2MP: H_2O ratio			3:3:1

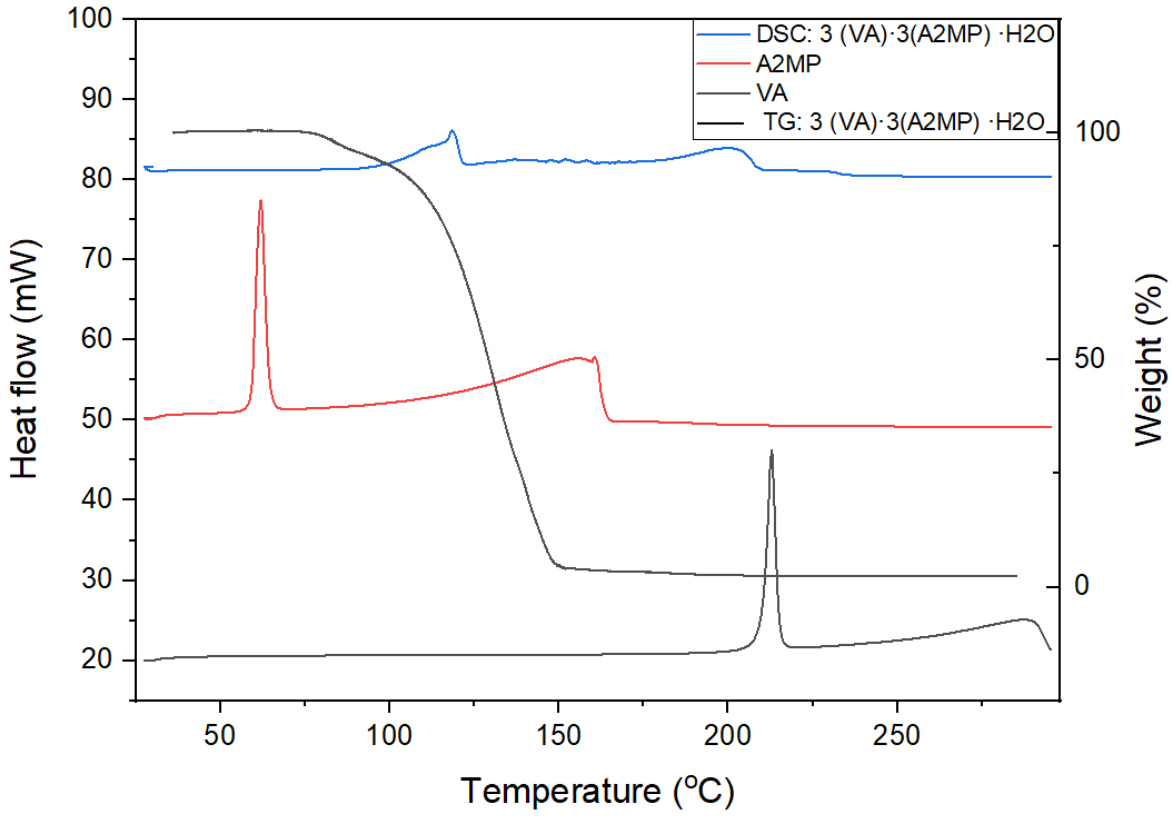

Figure 5.4: Thermal analysis curves: DSC of $3(VA^{-})3(A2MP^{+})\cdot H_2O$ (blue), A2MP (red), VA (black), TG: $3(VA^{-})3(A2MP^{+})\cdot H_2O$ (black).

5.2.3 Powder X-ray diffraction

Vanillic acid and 2-aminopyridine were ground in a 1:1 ratio with and without solvent for 30 minutes. Powder X-ray diffraction (PXRD) spectra were compared to those of the single crystal and the calculated pattern of $3(VA^{-})3(A2MP^{+})\cdot H_2O$ acquired from Mercury. The PXRD patterns from the grinding trials complied with the calculated and single crystal patterns. Peaks at 2θ = 12.5 and 27.1 ° in both ground products are more evident than those in calculated and single crystal patterns. The PXRD signals from all the studies used to describe the salt hydrate are presented in Figure 5.5.

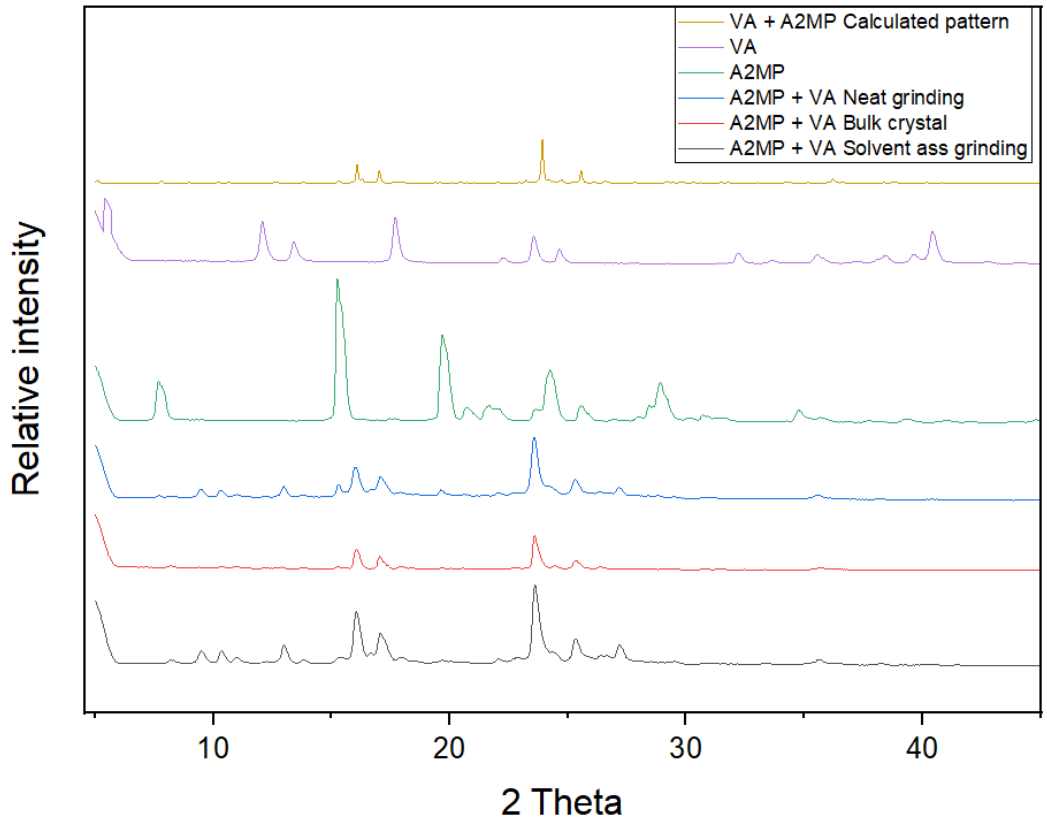

Figure 5.5: PXRD patterns of calculated pattern of $3(VA^{-})3(A2MP^{+})\cdot H_2O$ (yellow), VA (purple), A2MP (green), ground product (blue), bulk crystal (red), solvent assisted ground product (black).

5.2.4 Structure determination

The salt hydrate $3(VA^{-})3(A2MP^{+})\cdot H_2O$ crystallized in a 3:3:1 stoichiometry and formed yellow block-like crystals. The structure was solved using direct methods in the monoclinic space group $P2_1/n$. The crystal data is given in Table 5.3.

Table 5.3: Crystal data and refinement parameters of the 3(VA⁻)3(A2MP⁺)·H₂O salt.

Compound	**3(VA⁻)3(A2MP⁺)·H₂O**
Structural formula	3($C_8H_7O_4^-$)3($C_5H_7N_2$)·(H_2O)
Ratio	3:3:1
M_r (g mol^{-1})	804.80
Temperature (K)	173
Crystal system	monoclinic
Space group	$P2_1/n$
a (Å)	9.5093(19)
b (Å)	11.970(2)
c (Å)	34.732(7)
α (°)	90
β (°)	93.75(3)
γ (°)	90
Volume (Å^3)	3945.0(14)
Z	4
D_c, Calc density (g cm^{-3})	1.355
Final R indices [I>2 σ (I)]	R_1 = 0.0417 wR_1 = 0.0973
R indices (all data)	R_2 = 0.0604 wR_2 = 0.1076
Largest diff. peak and hole (eÅ^{-3})	0.658; -0.248

3(VA⁻)3(A2MP⁺)·H₂O exhibits a variety of hydrogen bonds involving nitrogen, including N_{pyr}^+-H···O⁻ (pyridinium carboxylate synthon), N⁺-H···O⁻ (amine carboxylate synthon), and also O-H···O hydrogen bonds involving methoxy groups and alcohol groups. The hydrogen bond data are summarized in Table 5.4. There are a number of ring formations in the structure; $R_2^2(8)$ rings between 2-aminopyridinium and vanillate, $R_4^4(20)$ and $R_4^4(18)$ rings between two vanillate anions and two water molecules, and $R_1^2(5)$ rings between one vanillate anion and one water molecule. The VA⁻ anions are connected via O-H···O hydrogen bonding forming $C_1^1(8)$ and $C_2^2(16)$ chains. The hydrogen bonds are shown in Figure 5.6.

Table 5.4: Geometrical data for hydrogen bond of 3(VA^-)3($A2MP^+$)·H_2O.

Compound	D-H···A	D···A (Å)	D-H (Å)	H···A (Å)	D-H···A (°)	Symmetry operations
3(VA^-3($A2MP^+$)·H_2O	N1-H94…O5	2.6390(16)	0.97(2)	1.68(2)	171.0(18)	x, y, z
	N2-H13A…O6	2.8353(18)	0.897(19)	1.943(19)	172.9(17)	$x, 1+y, z$
	N2-H13B…O13	2.9814(19)	0.908(18)	2.074(19)	178.8(16)	x, y, z
	N3-H105…O2	2.6081(15)	0.974(18)	1.636(18)	175.6(16)	$x, y-1, z$
	N4-H90A…O1	2.8274(17)	0.923(19)	1.905(19)	176.8(16)	$x, y-1, z$
	N4-H90B…O5	2.8556(17)	0.893(18)	1.971(18)	170.1(16)	$\frac{3}{2}-x, \frac{1}{2}+y, \frac{1}{2}-z$
	N5-H35A…O3	3.0672(17)	0.91(2)	2.21(2)	156.8(17)	$1+x, y, z$
	N5-H35B…O11	2.7827(17)	0.924(18)	1.862(18)	174.3(15)	$1+x, y, z$
	N6-H102…O12	2.6897(16)	0.919(19)	1.776(19)	172.6(17)	$1+x, y, z$
	O3-H5…O1	2.6238(14)	0.921(19)	1.72(2)	166.4(17)	$\frac{1}{2}-x, y-\frac{1}{2}, \frac{1}{2}-z$
	O9-H95…O6	2.6390(14)	0.923(19)	1.722(19)	172.1(17)	x, y, z
	O7-H21…O11	2.6545(14)	0.91(2)	1.78(2)	160.7(18)	$1+x, y, z$
	O13-H108…O10	2.8900(16)	0.88(3)	2.19(3)	135(2)	$1-x, -y, -z$
	O13-H109…O12	2.9609(17)	0.95(2)	2.02(2)	173.5(19)	x, y, z

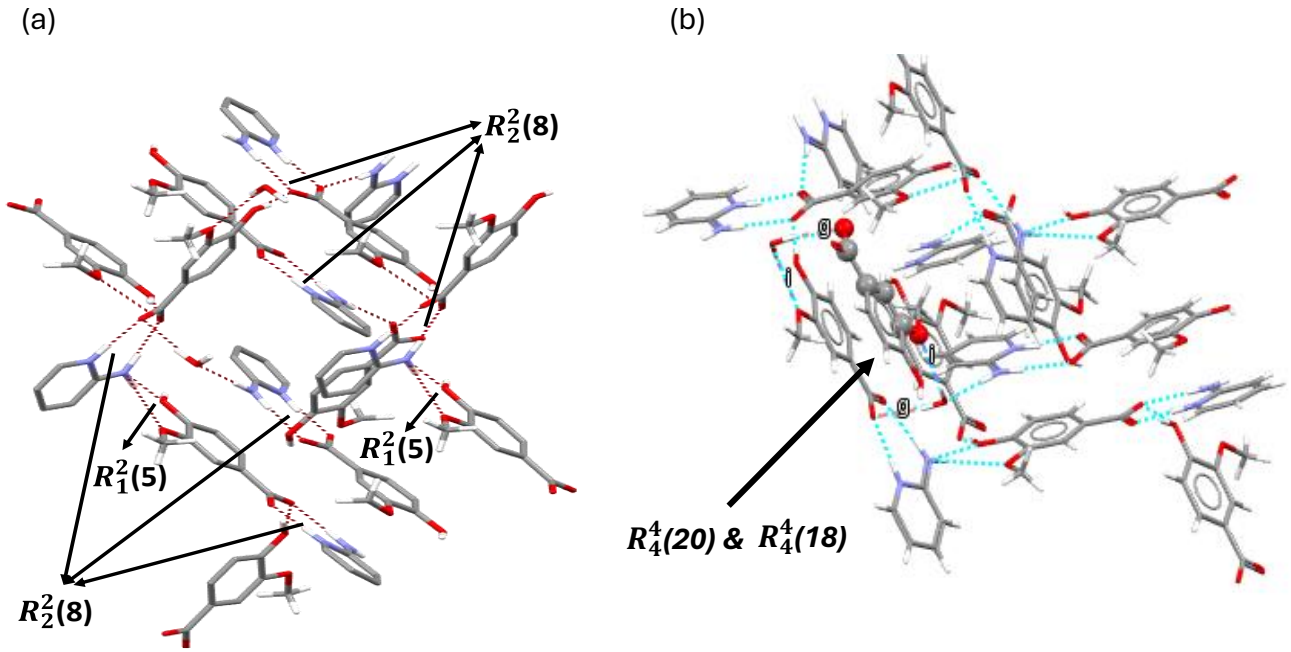

Figure 5.6: Hydrogen bonding of 3(VA⁻)3(2AMP⁺)·H_2O.

The structure has weak contacts, including a face-to-face π-π stacking interaction between neighbouring A2MP cations with a centroid distance of 3.7555(8) Å and between A2MP cations and VA anions with a Cg-Cg = 3.7737(8) Å. Another weak interaction in the form of C-H···π occurs between the methyl group (C34-H34) of VA and another VA ring (C27-C32) at 3.6766(7) Å. VA, A2MP, and water molecules form chains perpendicular to the a-axis. Figures 5.7 and 5.8 depict respectively the packing diagram for the salt hydrate and the cavities inhabited by water molecules, with a void volume of 99.69 $Å^3$ (2.5% of unit cell), probe radius of 1.2 Å, and grid spacing of 0.3 Å (contact surface).

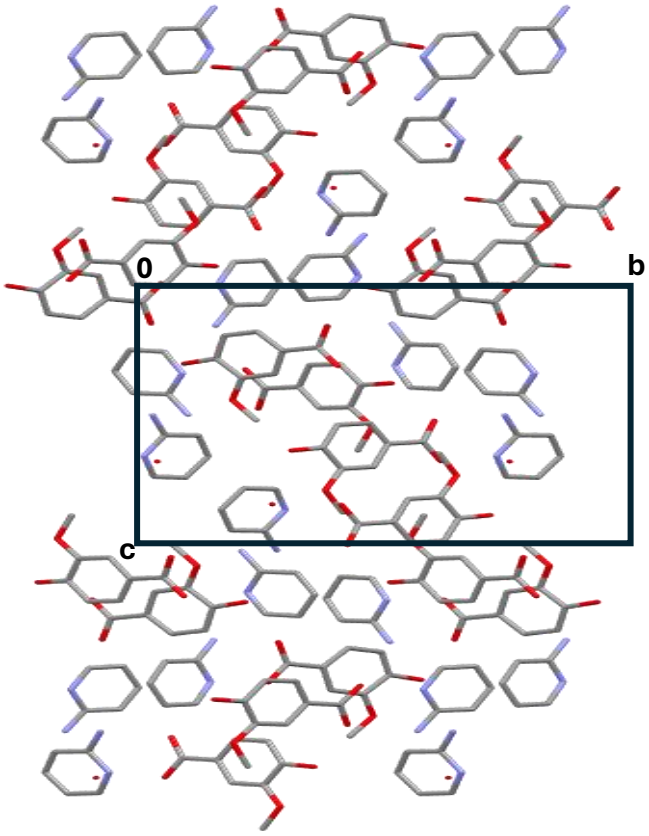

Figure 5.7: Packing diagram of 3(VA^-)·3($2AMP^+$)·H_2O (hydrogens have been omitted for clarity).

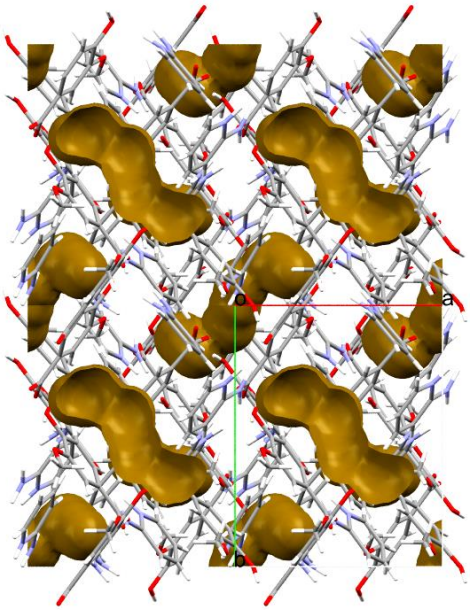

Figure 5.8: Cavities in which water molecules are located.

5.3 Vanillic acid and 4-aminopyridine ($(VA^-)(A4MP^+)\cdot 2H_2O$)

4-aminopyridine (A4MP) is a hygroscopic white crystalline solid, that has been used as a medicine to control some of the symptoms of multiple sclerosis and is approved for symptomatic improvement of walking in individuals with various forms of the disease (Korenke et al., 2008). The vanillate 4-aminopyridinium salt hydrate depicted in Figure 5.9 was prepared by dissolving 50 mg of vanillic acid and 29 mg of 4-aminopyridine in 2 ml of ethanol in a 1:1 molar ratio (0.3 mmol). The concentrated solution was allowed to crystallize through slow evaporation at room temperature, and crystals formed after two days. The $(VA^-)(A4MP^+)\cdot 2H_2O$ structure crystallized in $P2_1$ with one vanillate anion, one 4-aminopyridinium cation, and two water molecules in the asymmetric unit (Figure 5.9) forming colourless block-like crystals.

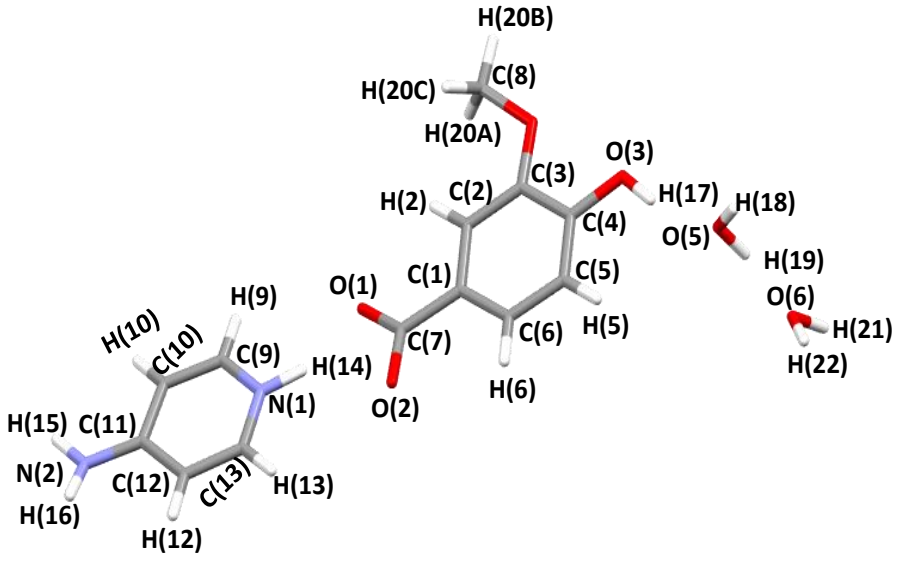

Figure 5.9: Asymmetric unit of the $(VA^-)(A4MP^+)\cdot 2H_2O$ structure with all the hydrogen atoms shown for numbering clarity.

5.3.1 FTIR spectroscopy

When a carboxylic acid is deprotonated, it forms a carboxylate moiety (COO^-). The carboxylate bands are commonly observed between 1400 and 1600 cm^{-1}. The main bands were determined, and the corresponding changes were recorded. The FTIR spectra of VA, plotted

with its salt (Figure 5.10), indicates the existence of the distinctive peak at 3482 cm^{-1} allocated to the O-H of the carboxylic acid and 1663 cm^{-1} assigned to the conjugated carbonyl (C=O). The FTIR spectra of the $(VA^{-})(A4MP^{+})\cdot 2H_2O$ salt hydrate displays two weak, slightly broad bands at 3393-3343 cm^{-1}, corresponding to the main amine (NH_2) of the coformer that is hydrogen bonded to the carboxylate of VA. The carbonyl group shows a shift at 1598 cm^{-1} as a result of hydrogen bonded intermolecular interactions with the coformer's amine. Table 5.5 displays the positions and assignments of main peaks in VA, A4MP and $(VA^{-})(A4MP^{+})\cdot 2H_2O$ salt hydrate.

Table 5.5: FTIR positions and assignments of peaks in VA, A4MP and $(VA^{-})(A4MP^{+})\cdot 2H_2O$.

VA	**A4MP**	**$(VA^{-})(A4MP^{+})\cdot 2H_2O$**	**Proposed assignments**
3482	-	3218	O-H stretch
1663	-		C=O
-	-	1598	COO^{-}
1276, 1209			C-O stretch
-	3434, 3297	3393, 3343	N-H stretch
	1647	1604	$-NH_2$ bend

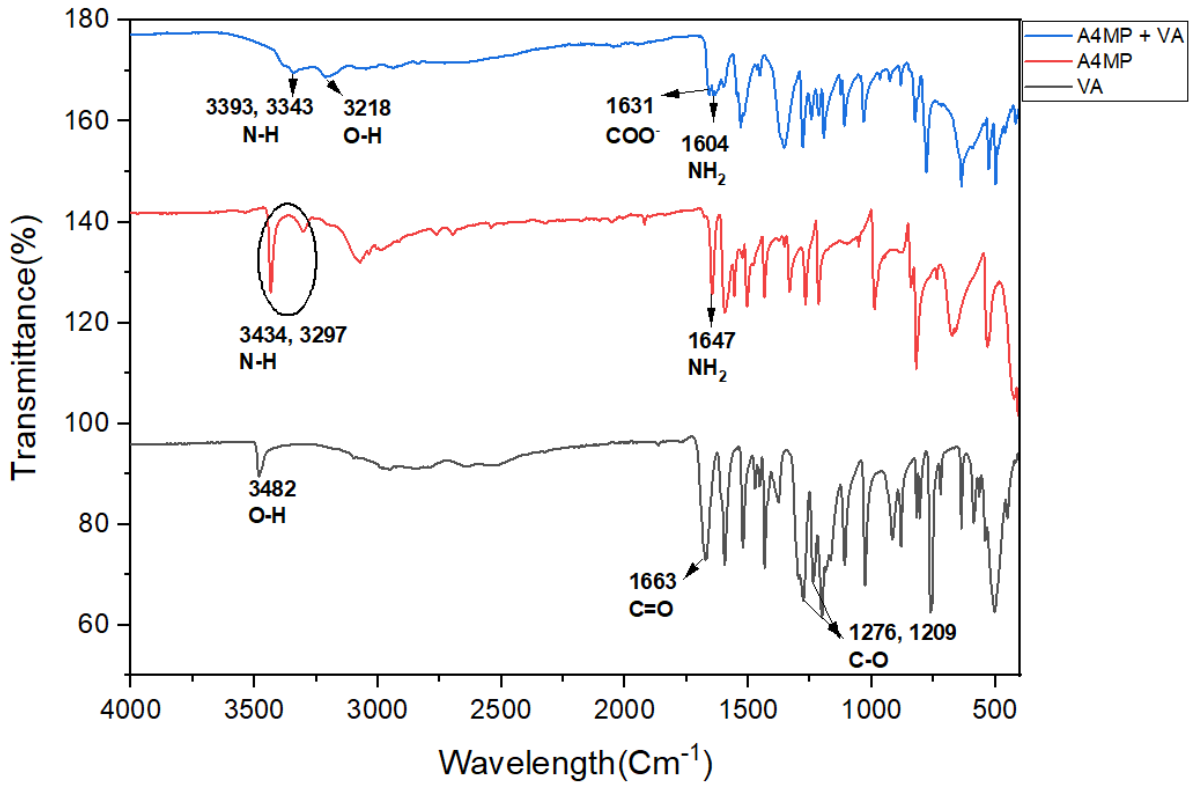

Figure 5.10: FTIR spectra of VA (black), A4MP (red) and $(VA^-)(A4MP^+)\cdot 2H_2O$ (blue).

5.3.2 Thermal analysis

There is good agreement between the experimental and computed percentage mass losses for the TG data. The thermal analysis results are presented in Table 5.6. The TG curve shows three mass losses: the first two result in the loss of 2 moles of water, for a total mass loss percentage of 12.21 % and the calculated mass loss was 12.19 %. The salt hydrate's DSC curve shows two endotherms: the first corresponds to the melt of the salt and the release of water, while the second corresponds to salt decomposition. Figure 5.11. shows the thermal analysis results.

Table 5.6: Thermal analysis data for $(VA^-)(4AMP^+)\cdot 2H_2O$.

Compounds	**Vanillic acid**	**4-aminopyridine**	**(VA^-) $(A4MP^+)\cdot 2H_2O$**
DSC $_{Endo1}(T_{onset}$,°C)	213	162	105
DSC $_{Endo2}(T_{onset}$,°C)			198
TG calc % mass loss			12.19
TG exp % mass loss	-	-	12.21
VA: A4MP: H_2O ratio			1:1:2

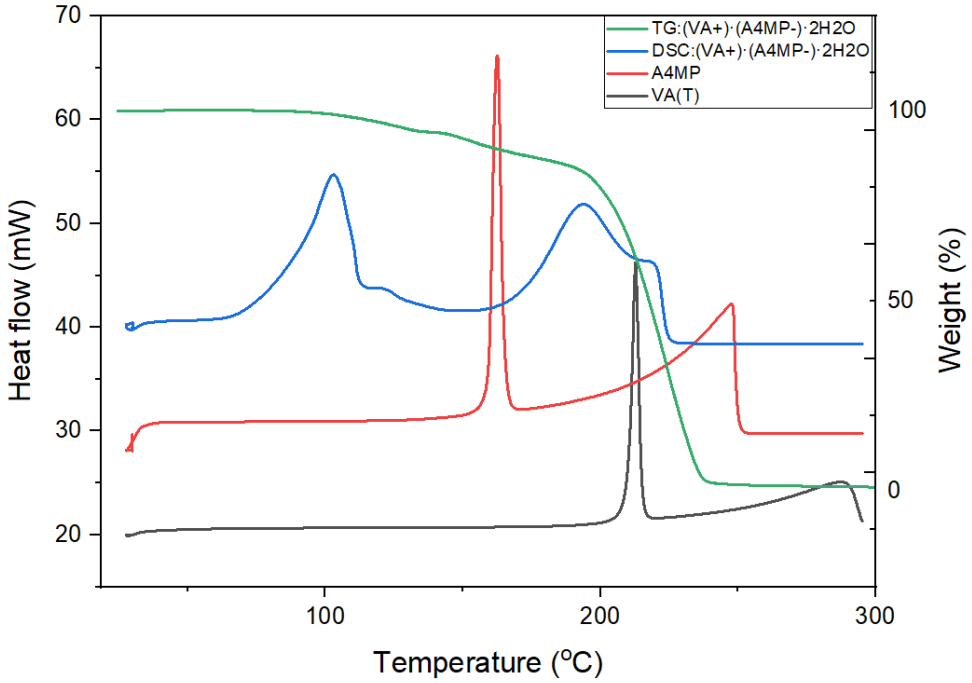

Figure 5.11: DSC curves of Vanillic acid (blue), A4MP (orange), $(VA^-)(A4MP^+)\cdot 2H_2O$ (red) and TG curve of $(VA^-)(A4MP^+)\cdot 2H_2O$.

5.3.3 Powder X-ray diffraction

The PXRD patterns of the solvent assisted ground product, the bulk crystal, and the calculated pattern from Mercury are all in good agreement. However, the PXRD pattern of the neat ground product did not completely match either the solvent assisted ground product, the bulk crystal, or the calculated PXRD patterns. It was concluded that the neat grinding experiment resulted in a partial conversion of the product. Figure 5.12 displays PXRD patterns for all different experiments.

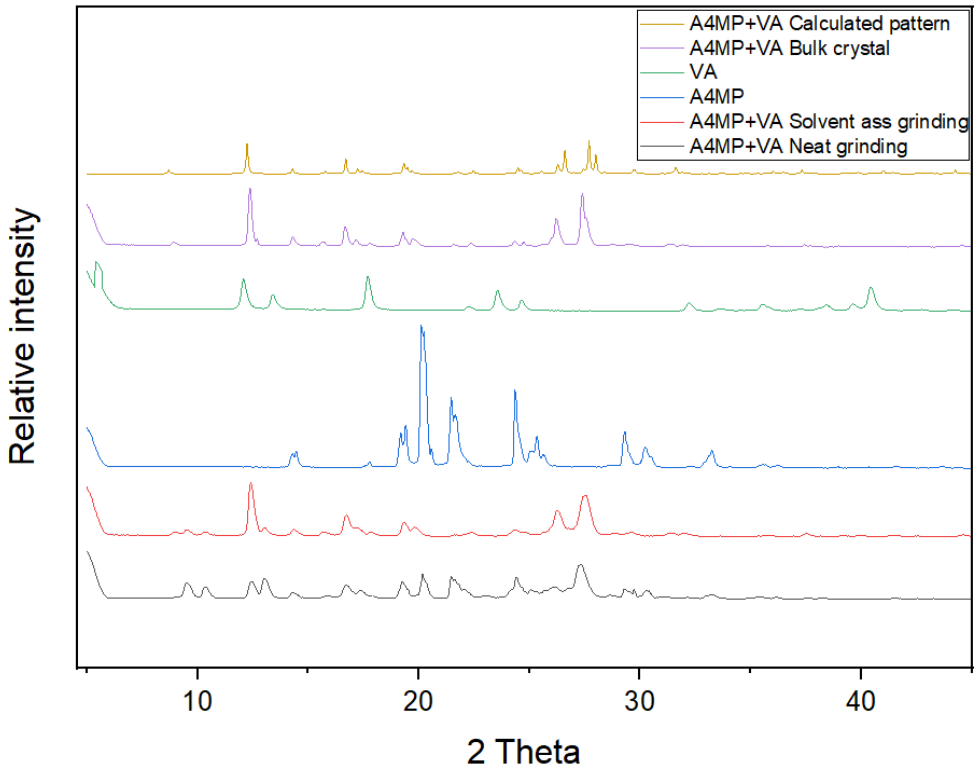

Figure 5.12: $(VA^{-})(A4MP^{+})\cdot 2H_2O$ calculated pattern (yellow), $(VA^{-})(A4MP^{+})\cdot 2H_2O$ bulk crystal (purple), VA (green), A4MP (blue), solvent assisted ground product (red), neat ground product (black).

5.3.4 Structure Determination

The salt hydrate of $(VA^{-})(A4MP^{+})\cdot 2H_2O$ was a yellow block like crystal and the structure was solved in the monoclinic space group $P2_1$, using direct methods and refined using full matrix least squares with SHELX refining on F^2. The crystal data parameters are displayed in Table 5.7 below.

Table 5.7: $(VA^{-})(A4MP^{+})\cdot 2H_2O$ crystal data.

Compound	**$(VA^{-})(A4MP^{+})\cdot 2H_2O$**
Structural formula	$C_8H_7O_4.C_5H_7N_2.2H_2O$
Ratio	1:1:2
M_r ($gmol^{-1}$)	298.29
temperature (K)	173 K
Crystal system	monoclinic
Space group	$P2_1$
a (Å)	6.8360(14)
b (Å)	10.282(2)
c (Å)	10.361(2)
α (°)	90
β (°)	101.59(3)
γ (°)	90
Volume (Å3)	713.4(3)
Z	2
D_c, Calcd density (gcm^{-3})	1.389
Final R indices [I>2 σ (I)]	R_1 = 0.0496 wR_1 = 0.1435
R indices (all data)	R_2 = 0.0531 wR_2 = 0.1465
Largest diff. peak and hole ($eÅ^{-3}$)	0.383; -0.282

The $(VA^{-})(A4MP^{+})\cdot 2H_2O$ structure exhibits intermolecular coplanar alignment (π-π stacking). A π- π stacking interaction exists between the vanillic acid aromatic ring (C1-C6) and the six-membered ring of the 4-aminopyridine (N1-C13), with a distance between centroids of 3.5319 Å. VA and A4MP are packed in layers and form chains parallel to the b axis (Figure 5.13). Figure 5.14 depicts the cavities occupied by water molecules, with a void volume of 65.35 $Å^3$ (9.2 % of the unit cell), probe radius of 1.2 Å, and grid spacing of 0.3 Å (contact surface) (Macrae, 2020).

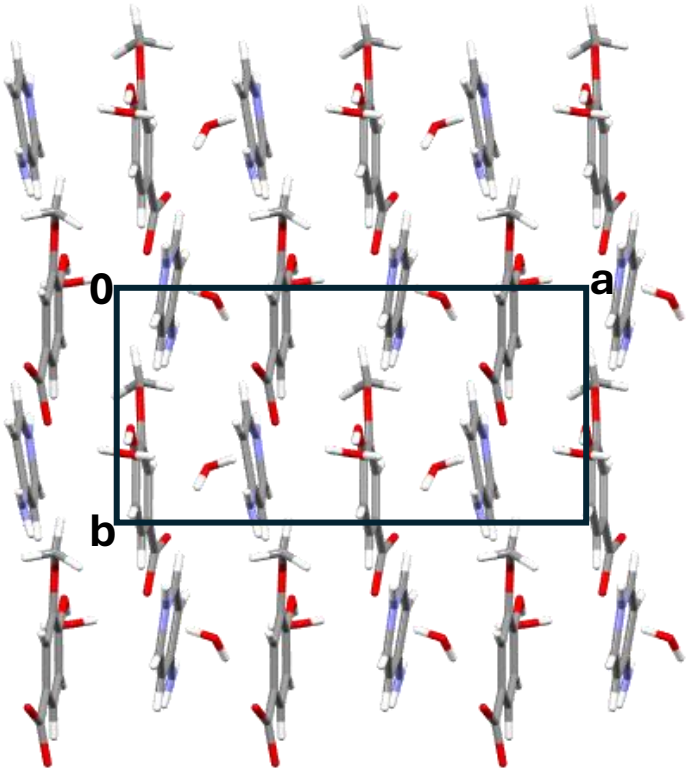

Figure 5.13: Packing diagram of (VA^-)($A4MP^+$)·$2H_2O$.

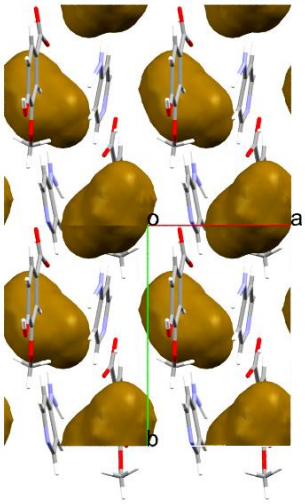

Figure 5.14: Cavities in which water molecules are located.

The structure is distinguished by its highly complicated hydrogen bonding. The hydrogen bond network uses all donor/acceptor sites of vanillic acid and 4-aminopyridine (Table 5.8). The N-H···O and O-H···O interactions form strong hydrogen bonds.

The two water molecules in the structure with oxygens, O5 and O6 act as bridging molecules, linking two vanillate anions, whereas the water molecule with O6 connects two vanillate anions with a 4-aminopyridinium cation. Jacobs et al reported on this type of hydrogen bonding in which water acts as a bridge (Jacobs et al., 2013).

In the crystal structure, each vanillate anion is hydrogen bonded to four water molecules and two 4-aminopyridinium cations. (VA^-)($A4MP^+$)·$2H_2O$ has three hydrogen bonds involving nitrogen; one N_{pyr}^+-H···O^- (pyridinium carboxylate synthon), and two N^+-H···O^- (amine carboxylate synthon). The structure includes O-H···O hydrogen bonds between the carboxylate and alcohol of vanillic acid, as well as water (Table 5.8). The structure is also characterized by $R_1^2(5)$ and $R_1^2(4)$ rings that connect vanillate anions and 4-aminopyridinium cations. The $A4MP^+$ cations are linked together through a VA^- anion via N^+-H···O^- hydrogen bonds forming $C_2^2(10)$, $C_2^2(13)$ and $C_2^2(14)$ chains. Two water molecules are linked together through VA^- via O^+-H···O^- hydrogen bonds forming $C_2^2(6)$ chains. The hydrogen bonding is shown in Figure 5.15.

Table 5.8: Geometrical data for hydrogen bond of (VA^-)($A4MP^+$)·$2H_2O$.

Compound	**D-H···A**	**D···A (Å)**	**D-H (Å)**	**H···A (Å)**	**D-H···A (°)**	**Symmetry operations**
(VA^-)($A4MP^+$)·$2H_2O$	N1-H14···O1	2.736(4)	0.98(7)	1.80(7)	159(6)	x, y, z
	O6-H21···O2	2.796(4)	0.91(6)	1.92(7)	159(6)	$-x, y-\frac{1}{2}, 1-z$
	N2-H15···O6	2.987(4)	0.92(4)	2.13(4)	154(4)	$-x, \frac{1}{2}+y, -z$
	N2-H16···O3	3.028(4)	0.85(6)	2.20(6)	166(5)	$x, 1+y-, z-1$
	O5-H19···O6	2.807(4)	0.91(3)	1.90(3)	173(8)	x, y, z
	O3-H17···O5	2.612(4)	0.88(7)	1.76(7)	164(6)	x, y, z
	O6-H22···O1	2.720(4)	0.83(7)	1.90(7)	166(6)	$x, y, 1+z$
	O5-H18···O2	2.783(4)	0.81(10)	2.00(10)	162(9)	$1-x, y-\frac{1}{2}, 1-z$

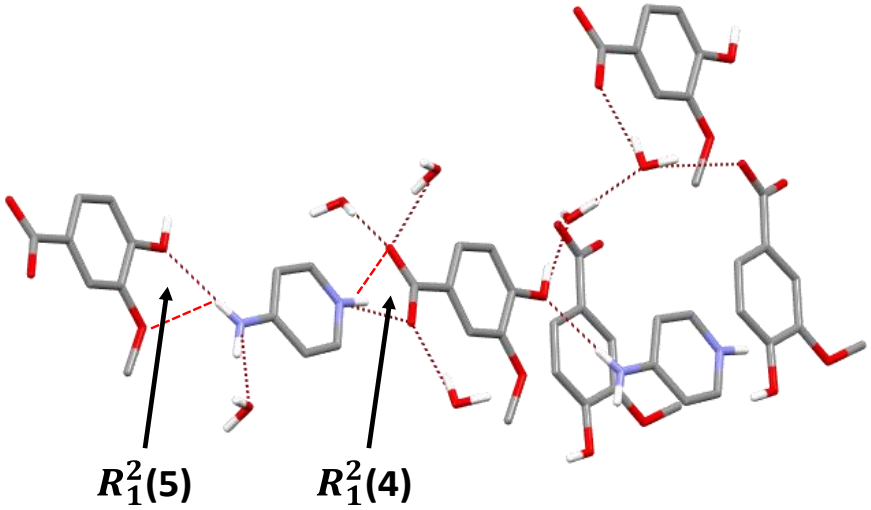

Figure 5.15: Hydrogen bonding of $(VA^-)(A4MP^+)\cdot 2H_2O$.

5.4 Summary

2-aminopyridine and 4-aminopyridine being hygroscopic compounds, they absorb moisture in the atmosphere resulting in the formation of salt hydrates. Two salt hydrates were successfully identified, confirming the pK_a rule. The new solid forms were investigated using single crystal X-ray diffraction. Both structures were solved in the monoclinic crystal system: space group $P2_1/n$ for $3(VA^-)3(A2MP^+)\cdot H2O$ and $P2_1$ for $(VA^-)(A4MP^+)\cdot 2H_2O$.

For both structures, water forms a bridge between molecules through hydrogen bonds. FTIR spectroscopy also clearly demonstrates the presence of a band corresponding to the anion carboxylate in the spectra of both salt hydrate forms. The DSC results show that the salt hydrate $3(VA^-)3(A2MP^+)\cdot H_2O$ is more stable than $(VA^+)(A4MP^-)\cdot 2H_2O$. In the case of vanillic acid and 2-aminopyridine, the PXRD patterns from both grinding experiments matched well with the PXRD pattern from the bulk crystal and the calculated pattern from Mercury. However, the PXRD pattern from the neat grinding experiment of vanillic acid and 4-aminopyridine revealed a partial conversion of the product.

REFERENCES

Clarke, H. D. et al. 2010. Structure-stability relationships in cocrystal hydrates: Does the promiscuity of water make crystalline hydrates the nemesis of crystal engineering. *Cryst Growth and Des*, 10(5): 2152–2167.

Gillon, A. L.; Feeder, N.; Davey, R. J. and Storey, R. 2003. Hydration in molecular crystals - A Cambridge Structural Database analysis. *Cryst Growth and Des*, 3(5): 663-673.

Jacobs, A., Amombo Noa, F. M. and Taljaard. J. H. 2013. J. *Chem. Crystallogr*. 43, 554 - 560.

Korenke, A.R.; Rivey, M.P. and Allington, D.R. 2008. Sustained-release fampridine for symptomatic treatment of multiple sclerosis. *The Annals of Pharmacotherapy*. 42 (10): 1458–1465.

Onder, E. and Sarier, N. 2015. Thermal regulation finishes for textiles. In: Paul R, editor. Functional finishes for textiles. Improving comfort, performance and protection. Amsterdam: *Elsevier*; pp. 17–98.

Serajuddin, A.T.; Pudipeddi, M.; Stahl, P.H. and Wermuth, C.G, editors. 2002. Handbook of pharmaceutical salts. *Weinheim: Wiley-VCH*; p. 138.

Shimizu, S.; Watanabe, N.; Kataoka, T.; Shoji, T.; Abe, N.; Morishita, S. and Ichimura, H. 2007. Pyridine and Pyridine Derivatives. Ullmann's Encyclopedia of Industrial Chemistry. *Weinheim: Wiley-VCH*.

CHAPTER 6: SUMMARY AND CONCLUSION

The synthesis of multicomponent crystals has a lot of benefits in the pharmaceutical and food industries as the solids obtained generally have better physicochemical properties like solubility and bioavailability than their corresponding parents' compounds. When forming a cocrystal, salt or solvate, the functional groups of both the starting material and the coformer can be used to predict the development of multicomponent crystals, as well as the pK_a rule, which determines the formation of cocrystals or salts.

Vanillic acid can form heterosynthons and homosynthons due to its carboxylic acid, hydroxyl and methoxy groups. This study successfully synthesized five novel solid forms using vanillic acid (VA) as the starting material and several organic bases as coformers. Addiitonal experiments were also done to characterise a sixth solid form that was previously reported. The crystals were produced using slow evaporation procedures, and the neat and solvent-assisted grinding process was utilized to test their repeatability.

The solvent assisted grinding experiment was successful for the VA·4,4-BP cocrystal, however the neat grinding experiment resulted in partial reaction. For the (VA^-)(4DMAP$^+$) salt neither the solvent assisted griding nor the neat grinding experiments were successful. For the (VA^-)(A25MP$^+$) salt, both grinding experiments resulted in a physical mixture of the starting materials. For the (VA^-)(A26MP$^+$) salt, both experiments resulted in the partial conversion of the products. For the 3(VA^-)3(A2MP$^+$)·H_2O salt hydrate, the grinding experiments were successful, all the PXRD patterns from the grinding experiments matched the calculated pattern from Mercury and the bulk crystal pattern. For the (VA^-)(A4MP$^+$)·2H_2O salt hydrate, the solvent assisted grinding experiment was successful, however the neat grinding experiment resulted in a partial conversion of the product.

The crystal structure of VA and 4,4-bipyridine was solved in the monoclinic space group $P2_1/c$. The VA·4,4-BP cocrystal had a Z value of 4. The structure is characterized by O-H···N hydrogen bonding between VA^- anions and 4,4-BP$^+$ cations, forming $C_2^2(17)$ chains in the packing diagram. Although this structure has previously been reported in the literature, this study characterised the cocrystal using additional methods of thermal analysis and FTIR spectroscopy.

The pK_a rule was proven valid because the pK_a difference between the starting material and 4,4-BP indicated cocrystal formation. Thermal analysis established the formation of VA·4,4-BP with a different melting point than the initial compounds. The pK_a rule was confirmed for VA salts, as the ΔpK_a between acids and bases fell within the range for salt formation. Proton transfer in the crystal structures proved this result.

The crystal structures of VA with 4DMAP and A25MP were solved in the monoclinic space groups $P2_1/n$ and $P2_1$ respectively while the A26MP crystal structure solved in the orthorhombic space group *P*bca. Only the (VA^-)($4DMAP^+$) structure involved OH and COO^- groups of VA in the formation of a heterosynthon with the pyridines while the (VA^-)($A25MP^+$) and (VA^-)($A26MP^+$) structures involved the 2-aminopyridinium carboxylate heterosynthon. Thermal analysis results revealed that the salt formed with 4DMAP was the most stable among the three salts formed.

The crystal structures of the VA salt hydrates were solved in different monoclinic space groups, $P2_1/n$ for $3(VA^-)3(A2MP^+)\cdot H_2O$ and $P2_1$ for $(VA^-)(A4MP^+)\cdot 2H_2O$. Both structures displayed the carboxylate amine heterosynthon resulting in $R_1^2(5)$ rings and $3(VA^-)3(A2MP^+)\cdot H_2O$ also featured the 2-aminopyridinium carboxylate heterosynthon. In both structures, water plays the bridging role thus connecting molecules within the crystals. The DSC analysis revealed that the salt hydrate formed with A2MP was more stable than the one formed with A4MP. Further studies should investigate the solubility and bioavailability of the cocrystals, salts and salt hydrates of VA. Additionally, the impact of molar ratio of the starting compounds and the choice of solvent can also be investigated.